Springer

Dear Author,

Here are the proofs of your article.

- You can submit your corrections **online**, via **e-mail** or by **fax**.
- For **online** submission please insert your corrections in the online correction form. Always indicate the line number to which the correction refers.
- You can also insert your corrections in the proof PDF and **email** the annotated PDF.
- For fax submission, please ensure that your corrections are clearly legible. Use a fine black pen and write the correction in the margin, not too close to the edge of the page.
- Remember to note the **journal title**, **article number**, and **your name** when sending your response via e-mail or fax.
- **Check** the metadata sheet to make sure that the header information, especially author names and the corresponding affiliations are correctly shown.
- **Check** the questions that may have arisen during copy editing and insert your answers/ corrections.
- **Check** that the text is complete and that all figures, tables and their legends are included. Also check the accuracy of special characters, equations, and electronic supplementary material if applicable. If necessary refer to the *Edited manuscript*.
- The publication of inaccurate data such as dosages and units can have serious consequences. Please take particular care that all such details are correct.
- Please **do not** make changes that involve only matters of style. We have generally introduced forms that follow the journal's style.
  Substantial changes in content, e.g., new results, corrected values, title and authorship are not allowed without the approval of the responsible editor. In such a case, please contact the Editorial Office and return his/her consent together with the proof.
- If we do not receive your corrections **within 48 hours**, we will send you a reminder.
- Your article will be published **Online First** approximately one week after receipt of your corrected proofs. This is the **official first publication** citable with the DOI. **Further changes are, therefore, not possible.**
- The **printed version** will follow in a forthcoming issue.

Please note

After online publication, subscribers (personal/institutional) to this journal will have access to the complete article via the DOI using the URL: http://dx.doi.org/[DOI].
If you would like to know when your article has been published online, take advantage of our free alert service. For registration and further information go to: http://www.link.springer.com.

Due to the electronic nature of the procedure, the manuscript and the original figures will only be returned to you on special request. When you return your corrections, please inform us if you would like to have these documents returned.

Metadata of the article that will be visualized in OnlineFirst

ArticleTitle	A homogenized structural model for shear deformable composites with compliant interlayers	
Article Sub-Title		
Article CopyRight	Springer Nature Switzerland AG (This will be the copyright line in the final PDF)	
Journal Name	Multiscale and Multidisciplinary Modeling, Experiments and Design	
Corresponding Author	Family Name	**Massabò**
	Particle	
	Given Name	**Roberta**
	Suffix	
	Division	Department of Civil, Chemical and Environmental Engineering, Polytechnic School
	Organization	University of Genova
	Address	Via Montallegro 1, 16145, Genoa, Italy
	Phone	+39010353-2956
	Fax	
	Email	roberta.massabo@unige.it
	URL	
	ORCID	
Author	Family Name	**Darban**
	Particle	
	Given Name	**Hossein**
	Suffix	
	Division	Department of Civil, Chemical and Environmental Engineering, Polytechnic School
	Organization	University of Genova
	Address	Via Montallegro 1, 16145, Genoa, Italy
	Phone	
	Fax	
	Email	
	URL	
	ORCID	
Schedule	Received	30 April 2018
	Revised	
	Accepted	20 August 2018

Abstract

Cylindrical bending of multilayered plates with thin compliant interlayers is studied through a homogenized structural model. The layers are homogeneous and orthotropic with principal material axes parallel and normal to the plane of bending and the interlayers are represented as sliding interfaces controlled by interfacial tractions which depend linearly on the relative displacements of the adjacent layers. The formulation is based on the zigzag theory formulated in Tessler et al. (J Compos Mater 43:1051–1081, https://doi.org/10.1177/0021998308097730, 2009) for fully bonded beams and the multiscale strategy in Massabò and Campi (Compos Struct 116:311–324, https://doi.org/10.1016/j.compstruct.2014.04.009, 2014), which is used to include the imperfect interfaces in the homogenized

	description of the problem. The kinematic variables are independent of the number of layers or imperfect interfaces and equal to four. The problem is solved in closed form on varying the interfacial stiffness between zero and infinite, which are the limiting values used to describe unbonded layers (traction-free interfacial sliding) and fully bonded layers (no sliding). The model accurately predicts global and local fields in highly anisotropic, simply supported, thick plates; some limitations are observed and discussed in the presence of in-plane material discontinuities and clamped supports. The model is applicable to study the elastic response of layered composites with adhesives interlayers or composite assemblies fastened by uniformly distributed mechanical connectors.
Keywords (separated by '-')	Structural theory - Laminated plate - Homogenization - Interface mechanics - Interlayer
Footnote Information	

Multiscale and Multidisciplinary Modeling, Experiments and Design
https://doi.org/10.1007/s41939-018-0032-x

ORIGINAL PAPER

A homogenized structural model for shear deformable composites with compliant interlayers

Hossein Darban[1] · Roberta Massabò[1]

Received: 30 April 2018 / Accepted: 20 August 2018

Abstract

Cylindrical bending of multilayered plates with thin compliant interlayers is studied through a homogenized structural model. The layers are homogeneous and orthotropic with principal material axes parallel and normal to the plane of bending and the interlayers are represented as sliding interfaces controlled by interfacial tractions which depend linearly on the relative displacements of the adjacent layers. The formulation is based on the zigzag theory formulated in Tessler et al. (J Compos Mater 43:1051–1081, https://doi.org/10.1177/0021998308097730, 2009) for fully bonded beams and the multiscale strategy in Massabò and Campi (Compos Struct 116:311–324, https://doi.org/10.1016/j.compstruct.2014.04.009, 2014), which is used to include the imperfect interfaces in the homogenized description of the problem. The kinematic variables are independent of the number of layers or imperfect interfaces and equal to four. The problem is solved in closed form on varying the interfacial stiffness between zero and infinite, which are the limiting values used to describe unbonded layers (traction-free interfacial sliding) and fully bonded layers (no sliding). The model accurately predicts global and local fields in highly anisotropic, simply supported, thick plates; some limitations are observed and discussed in the presence of in-plane material discontinuities and clamped supports. The model is applicable to study the elastic response of layered composites with adhesives interlayers or composite assemblies fastened by uniformly distributed mechanical connectors.

Keywords Structural theory · Laminated plate · Homogenization · Interface mechanics · Interlayer

1 Introduction

Layered composite structures, such as laminated and sandwich beams, plates, and shells, are largely used in aeronautical, aerospace, marine, energy, automotive, and civil applications, mostly because they can be tailored, by proper selection of materials and stacking sequences, to achieve unique properties, e.g., high strength-to-weight ratios, energy absorption, fatigue life, and environmental resistance. Typical composite laminates are made of fiber-reinforced polymer and ceramic or metallic layers; other examples of layered systems are cross-laminated timber, steel–concrete, and fiber-reinforced plastic–concrete assemblies and laminated glass.

The bonding between the plies in a layered structure may not always be strong enough to preserve the structural integrity and prevent relative displacements of the adjacent layers. This can be due to manufacturing defects, or to damage caused by in-service loads and environmental effects; or it can be a consequence of the presence of compliant elastic or inelastic interlayers. In layered wood or steel–concrete structures with layers joined by mechanical fasteners, such as nails, dowels, and screws, relative motion may occur due to elastic and inelastic mechanisms occurring within the connectors, the surrounding material, and their interface. In marine applications, bonding of the layers may weaken because of collisions with other marine vehicles or floating debris or waves slamming against the hull, or due to moisture ingress and sea-water effects (Penumadu 2018). The effective properties, global mechanical response, and local fields of layered structures are highly affected by the status of the bonding between the constitutive layers, see, for instance, (Goodman and Popov 1968; Vanderbilt et al. 1974; Foschi 1985), for experiments on layered wood beams and floors connected with mechanical fasteners, and (Jain and

✉ Roberta Massabò
roberta.massabo@unige.it

[1] Department of Civil, Chemical and Environmental Engineering, Polytechnic School, University of Genova, Via Montallegro 1, 16145 Genoa, Italy

Journal: 41939 MS: 0032 TYPESET DISK LE CP Disp.:2018/8/24 Pages: 21 Layout: Large

Mai 1994; Massabò et al. 1998; Cox 2005), for experiments and models on through-thickness reinforced laminates.

In this paper, a homogenized structural model is formulated for the linear static analysis of layered beams and plates in cylindrical bending with thin compliant interlayers. The model introduces zero-thickness interfaces in the zigzag theory formulated in Tessler et al. (2009) using the homogenization strategy proposed in Massabò and Campi (2014). The problem is described by a fixed number of displacement variables, independent of the number of layers, with advantages, both computational and analytical, over the most common approaches based on a discrete description of the problem. In the remaining of the "Introduction", different modeling approaches formulated to study layered structures with imperfect bonding will be discussed, with focus on the two models which will be used in this work, and the advantages and limitations of the model proposed here will be highlighted.

Thin interlayers in a layered structure can be modeled as regular discrete layers by directly accounting for their geometry and material properties in the analysis. However, this increases the number of unknown variables in analytical modeling and makes the solution computationally expensive for structures with many layers, also in the elastic regime. Moreover, the numerical description of thin interlayers is cumbersome and very fine discretizations are required. Similar difficulties are encountered when through-thickness connectors are represented explicitly in the numerical discretization of the problem. Special finite elements, theoretical and numerical techniques, and interface models have been formulated to describe interlayers, the action of distributed connectors or damaged interphases and delaminations and incorporate their effect into the analysis (Newmark et al. 1951; Adekola 1968; Goodman and Popov 1968; Murakami 1984; Carpenter and Barsoum 1989; Edlund and Klarbring 1990; Allix and Ladevèze 1992; Girhammar and Gopu 1993; Jain and Mai 1994; Bai and Sun 1995; Hansen and Spies 1997; Massabò et al. 1998; Mi et al. 1998; Adam et al. 2000; Heuer and Adam 2000; Alfano and Crisfield 2001; Andruet et al. 2001; Girhammar and Pan 2007; Xu and Wu 2007; Campi and Monetto 2013; Lenci et al. 2015). For layered structures with one or two in-plane dimensions much larger than the thickness, models have been formulated based on a priori assumptions on the through-thickness variation of the primary variables, typically the generalized displacements, using axiomatic approaches, e.g., equivalent single layer, layerwise, and zigzag theories (Abrate and Di Sciuva 2018). Equivalent single-layer theories are computationally simple, but unable to reproduce the complex stress and displacement fields which occur in layered structures due to the inhomogeneous material structure and the presence of compliant interlayers. Layerwise theories may accurately describe the mechanical response of highly anisotropic and relatively thick structures, also in the presence of thin interlayers or delaminations (Reddy 1987; Lu and Liu 1992; Andrews et al. 2006), at the expense of a large number of unknowns.

The zigzag theories offer a good compromise between computational simplicity and accuracy thanks to a multiscale treatment of the problem (Di Sciuva 2015; Abrate and Di Sciuva 2018). To describe structures with perfectly bonded layers, the global displacement field of an equivalent single-layer theory is enriched by through the thickness zigzag functions to account for the effects of the local inhomogeneous material architecture (Di Sciuva 1986, 1987; Murakami 1986; Cho and Parmerter 1993; Averill 1994; Aitharaju 1999; Tessler et al. 2009). The zigzag functions are then derived as functions of the global variables by imposing continuity conditions at the layer interfaces and field equations are obtained and solved in terms of the global variables only. The zigzag theory in Tessler et al. (2009) assumes the kinematics of the Timoshenko beam theory, which is enriched by an additional global variable and a piecewise linear zigzag function. The zigzag function is defined in terms of the global variables through continuity conditions on the shear tractions at the layer interfaces. The theory improves the description of the shear strains of the original theory in Di Sciuva (1986) leading to a better description of clamped supports, and is well suited for finite-element formulation, since it requires only C^0-continuous shape functions.

Thin interlayers can be represented in the homogenized approach of the zigzag theories as regular layers (Averill 1994) or zero-thickness interfaces. The latter approach, which was introduced in a number of papers in the literature in the 90s, was first solved in an energetically consistent way in Massabò and Campi (2014), for beams and wide plates, and in Massabò and Campi (2015), for general plates. The mechanical response of the interfaces is described through interfacial constitutive laws which relate the interfacial tractions to the relative displacements of the adjacent layers and may be used to approximate the response of thin interlayer. The models have been formulated for generally nonlinear interfacial traction laws, to describe mixed mode cohesive interfaces and delaminations. They couple a global equivalent single-layer theory and a local cohesive interface model through the introduction of zigzag functions which are piecewise linear in the thickness with discontinuities at the layer interfaces. The homogenization technique is similar to that of the classical zigzag theories and uses the assumed interfacial traction laws to equate the tractions at the layer surfaces to the interfacial tractions and relate them to the relative displacements of the layers. Models based on the homogenization strategy in Massabò and Campi (2014) have been used to accurately predicts local and global fields generated by thermo-mechanical loading in layered thick beams with continuous linear-elastic interfaces (Pelassa and Massabò 2015), to obtain approximate closed-form solutions of wave

Journal: 41939 MS: 0032 TYPESET DISK LE CP Disp.:2018/8/24 Pages: 21 Layout: Large

propagation problems (Massabò 2017) and fracture mechanics solutions for beams with mode II dominant traction-free delaminations (Darban and Massabò 2017a). One limitation of this homogenized approach for plates with fully debonded interfaces is the inability to account for the contribution of the shear deformations to the global transverse compliance; this is a consequence of the assumed interfacial continuity which implies zero transverse shear strains in beams, where the interfacial tractions vanish (see discussion later in the paper); in addition, fictitious boundary layers occur, under certain conditions, at the boundaries or at the crack tip cross sections (Massabò 2014; Pelassa and Massabò 2015), which complicate the solution of the problem.

In this paper, the zigzag theory in Tessler et al. (2009) is extended to account for the presence of zero-thickness linear-elastic interfaces following the approach in Massabò and Campi (2014). The model describes the linear-elastic regime of structures with thin compliant interlayers, e.g., adhesives, offering an efficient alternative to the zigzag models which treat the compliant interlayers as regular layers (Averill 1994). More importantly, the model is applicable to layered structures joined by uniformly distributed mechanical fasteners (nails, dowels, or screws), where the actual thickness of the interfaces is zero and classical zigzag approaches would not be applicable. The model maintains the advantages of the theory in Tessler et al. (2009) in the treatment of shear deformations thereby offering a solution to the limitations of the homogenized models which are based on the original zigzag functions, e.g., Di Sciuva's zigzag function, see list in Massabò and Campi (2014). The model yields closed-form solutions, in terms of four global displacement variables, for the asymptotic limit of fully debonded layers, which describes very compliant or fully damaged interlayers or the absence of mechanical connectors. The interfacial mechanisms are described by a single parameter, namely, the stiffness of the interfacial traction law; this allows to easily investigate and understand the effects of the status of the bonding on global and local fields and to define a global measure of the action developed by the interlayers/connectors which can be obtained, for instance, from in situ global measurements through the solution of an inverse problem. Some limitations of the approach in treating clamped supports and in-plane material discontinuities will be discussed in depth in the paper.

The formulation is limited to beams or plates in cylindrical bending and linear-elastic interfaces, which are assumed to be rigid against interfacial openings. It can be extended to model 2D structures and generally nonlinear interfaces following the methodology in Massabò and Campi (2015).

This paper is organized as follows. In Sect. 2, the problem is defined and the model assumptions are presented. In Sect. 3, the homogenized structural model is formulated and equilibrium equations are derived using a variational technique. In Sect. 4, the model is applied to study simply supported and cantilevered plates with different layups and interfacial conditions and its accuracy verified through comparison with elasticity solutions and structural mechanics discrete layer models; some limitations of the model in describing plates with in-plane discontinuities, e.g., finite length imperfect interfaces, and clamped supports are discussed. Conclusions are presented in Sect. 5.

2 Model assumptions

A multilayered wide plate is illustrated in Fig. 1a, with x_1–x_2–x_3 a system of Cartesian coordinates. The reference surface, S, is defined by the plane $x_3 = 0$ and the dimensions along x_1, x_2 and x_3 are L_1, $L_2 = L$ with $L_1 \gg L_2$, and h. The plate is subjected to static loads, which are independent of x_1 and act on the upper, S^+, lower, S^-, and lateral, B (with normal parallel to x_2) bounding surfaces. It is composed of n linearly elastic, homogenous, and orthotropic layers with principal material axes aligned along the coordinate axes. The layer k, with $k = 1, \ldots, n$ numbered from bottom to top, has thickness ${}^{(k)}h$ and lower and upper surfaces, ${}^{(k)}S^-$ and ${}^{(k)}S^+$, at the coordinates $x_3 = x_3^{k-1}$ and $x_3 = x_3^k$ [the superscripts (k) on the left and k on the right of a quantity show association with the layer k and with the interface between layers k and $k+1$, respectively]. The layers are joined by $n-1$ interfaces, which are zero-thickness mathematical surfaces, where the material properties and displacements may be discontinuous. The interfaces approximate the behavior of thin elastic interlayers or the elastic action of mechanical fasteners used to join individual layers. The plate deforms in cylindrical bending parallel to the plane x_2–x_3, Fig. 1b.

The layers are assumed to be incompressible in the thickness direction and the transverse normal stresses, ${}^{(k)}\sigma_{33}$, to be negligible compared to the other stress components. These assumptions are acceptable if the response is studied in regions far from boundaries, concentrated loads, or geometric discontinuities. The constitutive equations of the layer k are derived by particularizing the 3D constitutive equations to plane strain and imposing ${}^{(k)}\sigma_{33} = 0$. This yields, for $k = 1, \ldots, n$:

$$
\begin{aligned}
{}^{(k)}\sigma_{22} &= {}^{(k)}\bar{C}_{22}\,{}^{(k)}\varepsilon_{22},\\
{}^{(k)}\sigma_{23} &= {}^{(k)}C_{44}2\,{}^{(k)}\varepsilon_{23},
\end{aligned}
\tag{1}
$$

with ${}^{(k)}\sigma_{ij}$ and ${}^{(k)}\varepsilon_{ij}$, for $i, j = 2, 3$, the stress and strain components, and ${}^{(k)}\bar{C}_{22} = {}^{(k)}(C_{22} - C_{23}C_{32}/C_{33})$, where ${}^{(k)}C_{ij}$ for $i, j = 2, 3, 4$ are the coefficients of the stiffness matrix. The model presented in this paper is applicable to beams by replacing ${}^{(k)}\bar{C}_{22}$ with the Young's modulus in the x_2 direction and referring to the load acting per unit width.

Journal: 41939 MS: 0032 TYPESET DISK LE CP Disp.:2018/8/24 Pages: 21 Layout: Large

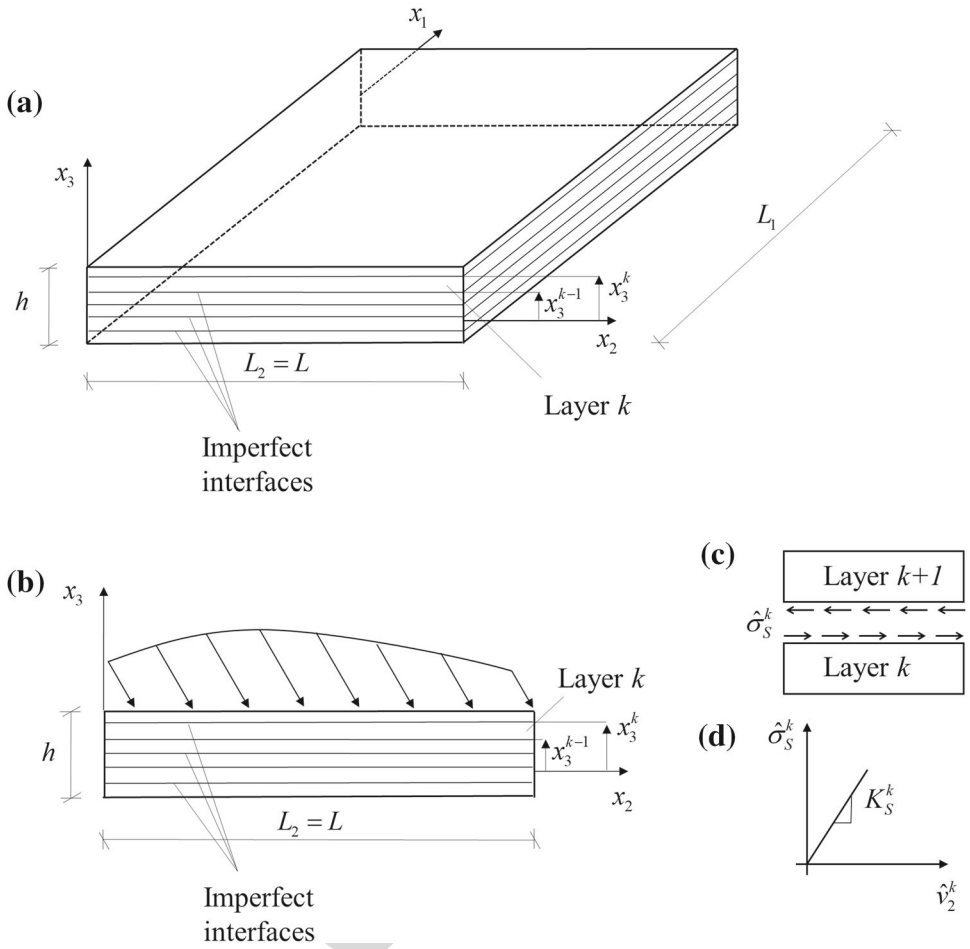

Fig. 1 **a** Multilayered wide plate with continuous imperfect or fully debonded interfaces. **b** Cross section in the plane x_2–x_3 with applied loads. **c** Interfacial tangential tractions $\hat{\sigma}_S^k$ acting on the surfaces of layers k and $k+1$. **d** Interfacial traction law

The mechanical behavior of the interface between the layers k and $k+1$ is described by a linear-elastic interfacial traction law, which relates the interfacial tangential tractions (Fig. 1c), $\hat{\sigma}_S^k(x_2)$, to the interfacial sliding jump:

$$\hat{v}_2^k(x_2, x_3 = x_3^k) = {}^{(k+1)}v_2(x_2, x_3 = x_3^k) - {}^{(k)}v_2(x_2, x_3 = x_3^k), \tag{2}$$

through

$$\hat{\sigma}_S^k(x_2) = K_S^k \hat{v}_2^k(x_2), \tag{3}$$

with K_S^k the interfacial tangential stiffness, Fig. 1d, and ${}^{(k)}v_2(x_2, x_3)$ the component of the displacement vector along the x_2-axis. The law with $K_S^k = 0$, which results in $\hat{\sigma}_S^k = 0$, describes fully debonded layers, and with $1/K_S^k = 0$, which results in $\hat{v}_2^k = 0$, represents fully bonded layers.

The assumed traction law well describes the response to shear loading of thin elastic interlayers, such as adhesive layers, in the absence of residual stresses. For a thin interlayer of thickness $\bar{h}$ and shear rigidity, ${}^{(\bar{k})}C_{44}$, the interfacial stiffness is $K_S = {}^{(\bar{k})}C_{44}/\bar{h}$. If the traction law in Eq. (3) is used to describe the initial elastic response of uniformly distributed mechanical fasteners, the interface stiffness depends on the geometrical and material properties of the connectors, the surrounding material and their interface. It can be determined experimentally, e.g., (Goodman and Popov 1968; Vanderbilt et al. 1974; Oehlers and Coughlan 1986), or through micromechanics modeling, as in Gelfi et al. (2002) for a stud embedded in a concrete–wood beam or in Cox (2005) for a through-thickness reinforcement embedded in a polymeric laminate. The linear-elastic law in Eq. (3) does not describe the nonlinear mechanisms related to damage and fracture of the interlayers or the nonlinear behavior of the connectors. To extend the model to describe nonlinear interfaces, the methodology formulated in Massabò and Campi (2014), which introduces piecewise linear cohesive traction laws, can be applied.

The interfaces are assumed to be rigid against relative opening displacements and the transverse displacements of the adjacent layers coincide at the interface, ${}^{(k)}v_3(x_3^k) = {}^{(k+1)}v_3(x_3^k)$. This assumption has been previously used in the literature, e.g., (Schmidt and Librescu 1996; Di Sciuva 1997; Di Sciuva et al. 2002), and is acceptable when the relative opening displacements at the interface are zero, due, for instance, to emisymmetric conditions, or negligible

Journal: 41939 MS: 0032 TYPESET DISK LE CP Disp.:2018/8/24 Pages: 21 Layout: Large

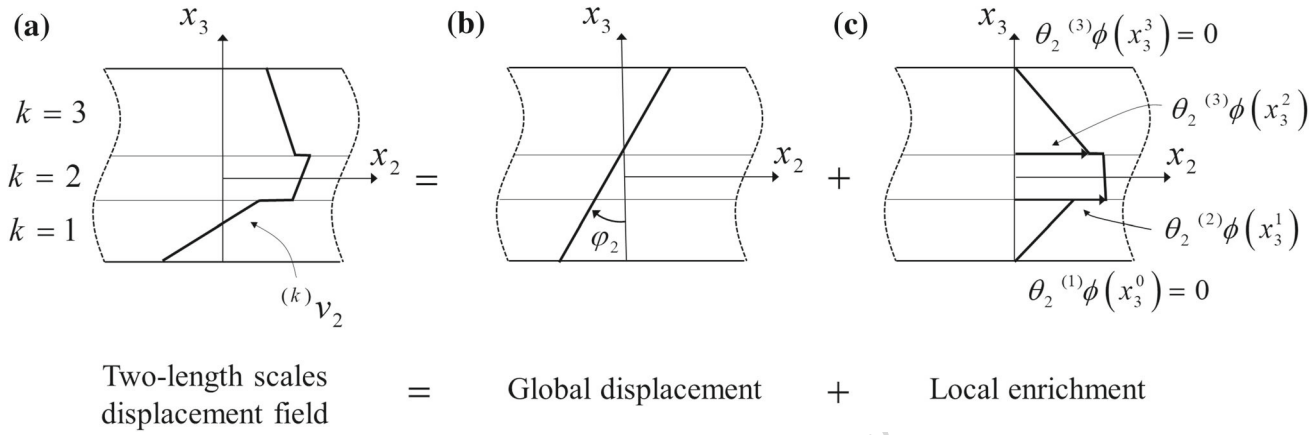

Fig. 2 Schematic description of the assumed displacement field in a three-layer laminate (**a**), global displacement (**b**), and local enrichment (**c**)

with respect to the sliding displacements due, for instance, to special loading/geometrical conditions. The assumption is acceptable when dealing with practical applications of laminated and composite plates, which often involve compressive transverse loads, for example, the hulls of marine vehicles.

3 Model formulation

3.1 Global and local variables and fields

Following the zigzag theory formulated in Tessler et al. (2009) for fully bonded beams and applying the methodology developed in Massabò and Campi (2014) to account for the presence of imperfect interfaces in a homogenized description of the problem, the longitudinal and transverse displacements in the layer k of the plate are assumed as (Fig. 2)

$$\begin{aligned} {}^{(k)}v_2(x_2, x_3) &= v_{02}(x_2) + x_3\varphi_2(x_2) + \theta_2(x_2)\,{}^{(k)}\phi(x_3), \\ {}^{(k)}v_3(x_2, x_3) &= w_0(x_2). \end{aligned} \tag{4}$$

The two-length scale field is controlled by four global variables, $v_{02}(x_2)$, $\varphi_2(x_2)$, $w_0(x_2)$, and $\theta_2(x_2)$. The first three, $v_{02}(x_2)$, $\varphi_2(x_2)$, and $w_0(x_2)$, correspond to a first-order shear deformation theory, Fig. 2b; if the reference surface coincides with the bottom or top surfaces of the plate, $v_{02}(x_2)$ is the longitudinal displacement of the reference surface, $\varphi_2(x_2)$ is the rotation of the normal to the reference surface, and $w_0(x_2)$ is the transverse displacement. The fourth global variable, $\theta_2(x_2)$, defines the variation along x_2 of a local enrichment function, ${}^{(k)}\phi(x_3)$, which is introduced to account for the inhomogeneous material structure and the presence of imperfect interfaces. The function ${}^{(k)}\phi(x_3)$ is independent of x_2 and assumed to be linear in the thickness of the layer and zero at the upper and lower surfaces of the plate (Fig. 2c):

$$\begin{aligned} {}^{(k)}\phi(x_3) &= {}^{(k)}\beta(x_3 - x_3^{k-1}) + {}^{(k)}\phi(x_3^{k-1})\frac{1}{2}, \\ {}^{(n)}\phi(x_3^n) &= {}^{(1)}\phi(x_3^0) = 0, \end{aligned} \tag{5}$$

with ${}^{(k)}\beta = {}^{(k)}\phi(x_3)_{,3}$ the slope and ${}^{(k)}\phi(x_3^{k-1})$ the value at the lower surface of the layer. The enrichment functions in the n layers of the plate define a local zigzag field which is piecewise linear with discontinuities at the layer interfaces, where in general, ${}^{(k)}\phi(x_3^k) \neq {}^{(k+1)}\phi(x_3^k)$, Fig. 2c.

The displacement field in Eq. (4) is defined by $2 \times (n-1)$ local unknowns, ${}^{(k)}\beta$ for $k = 1, \ldots, n$, and ${}^{(k)}\phi(x_3^{k-1})$ for $k = 2, \ldots n-1$, since ${}^{(1)}\phi(x_3^0) = 0$, ${}^{(n)}\phi(x_3^n) = 0$ and ${}^{(n)}\phi(x_3^{n-1}) = -{}^{(n)}\beta^{(n)}h$ after Eq. (5). The local unknowns will be defined as functions of the global variables through the imposition of continuity conditions at the layer interfaces in the next section.

The displacement field in Eq. (4) is similar to those assumed in the theories developed in Di Sciuva (1986, 1987) for fully bonded plates and in Massabò and Campi (2014) for plates with imperfect interfaces, which would be obtained by imposing the kinematic constraint $\theta_2(x_2) = \varphi_2(x_2) + w_{0,2}(x_2)$. The additional variable, $\theta_2(x_2)$, is introduced to better describe the transverse shear strains; this is useful, as it will be shown later, in problems with imperfect or fully debonded interfaces.

The strain and stress components in the layer k are derived using the displacement field in Eq. (4), linear compatibility and the constitutive Eq. (1):

$$\begin{aligned} {}^{(k)}\varepsilon_{22}(x_2, x_3) &= {}^{(k)}v_{2,2}(x_2, x_3) \\ &= v_{02,2}(x_2) + x_3\varphi_{2,2}(x_2) + \theta_{2,2}(x_2)\,{}^{(k)}\phi(x_3), \\ 2\,{}^{(k)}\varepsilon_{23}(x_2, x_3) &= {}^{(k)}v_{2,3}(x_2, x_3) + {}^{(k)}v_{3,2}(x_2, x_3) \\ &= \varphi_2(x_2) + w_{0,2}(x_2) + \theta_2(x_2)\,{}^{(k)}\beta. \end{aligned} \tag{6}$$

Journal: 41939 MS: 0032 TYPESET DISK LE CP Disp.:2018/8/24 Pages: 21 Layout: Large

$$
\begin{aligned}
{}^{(k)}\sigma_{22}(x_2, x_3) &= {}^{(k)}\bar{C}_{22}[v_{02,2}(x_2) + x_3\varphi_{2,2}(x_2) \\
&\quad + \theta_{2,2}(x_2){}^{(k)}\phi(x_3)], \\
{}^{(k)}\sigma_{23}(x_2, x_3) &= {}^{(k)}C_{44}[\varphi_2(x_2) + w_{0,2}(x_2) + \theta_2(x_2){}^{(k)}\beta].
\end{aligned} \tag{7}
$$

The bending strains and stresses are piecewise linear through the thickness and discontinuous at the interfaces. The transverse shear strains and stresses are piecewise constant; the strains depend on a global contribution, $\varphi_2 + w_{0,2}$, which is constant through the thickness and a local contribution, $\theta_2{}^{(k)}\beta$, which may differ in each layer. The transverse shear stresses can be rewritten as

$$
{}^{(k)}\sigma_{23} = {}^{(k)}C_{44}[(\varphi_2 + w_{0,2})(1 + {}^{(k)}\beta) + {}^{(k)}\beta(\theta_2 - \varphi_2 - w_{0,2})] \tag{8}
$$

which will prove useful in the following derivation.

The interfacial sliding jump at the interface k, $\hat{v}_2^k(x_2)$ in Eq. (2) is obtained from the displacement field in Eq. (4) as

$$
\hat{v}_2^k(x_2, x_3^k) = \theta_2(x_2)[{}^{(k+1)}\phi(x_3^k) - {}^{(k)}\phi(x_3^k)]. \tag{9}
$$

Equation (9) shows that when the layers are perfectly bonded to each other and $\hat{v}_2^k(x_2) = 0$, then ${}^{(k+1)}\phi(x_3^k) = {}^{(k)}\phi(x_3^k)$ and the zigzag contribution is C^0 continuous through the thickness. In this case, the displacement field is C^0 continuous, with discontinuous first derivatives and coincides with that of the original zigzag theory proposed in Tessler et al. (2009) for fully bonded beams. In the presence of imperfect interfaces, $\hat{v}_2^k(x_2) \neq 0$, ${}^{(k+1)}\phi(x_3^k) \neq {}^{(k)}\phi(x_3^k)$, and the displacement field is discontinuous at the interfaces.

Imposing the kinematic constraint $\theta_2(x_2) = \varphi_2(x_2) + w_{0,2}(x_2)$, the transverse shear stresses and relative displacements in Eqs. (8) and (9) would modify as

$$
\begin{aligned}
&{}^{(k)}\sigma_{23}(x_2, x_3) = {}^{(k)}C_{44}(\varphi_2 + w_{0,2})(1 + {}^{(k)}\beta) \\
&\hat{v}_2^k(x_2) = (\varphi_2 + w_{0,2})[{}^{(k+1)}\phi(x_3^k) - {}^{(k)}\phi(x_3^k)]
\end{aligned} \quad \text{for } \theta_2 = \varphi_2 + w_{0,2}, \tag{10}
$$

and coincide with the transverse shear stresses and relative displacements assumed in Massabò and Campi (2014).

3.2 Derivation of the enrichment functions

The local variables in Eqs. (4) and (5), ${}^{(k)}\beta$ for $k = 1, \ldots n$, and ${}^{(k)}\phi(x_3^{k-1})$ for $k = 2, \ldots n-1$, are defined in terms of the global variables following the procedure formulated in Tessler et al. (2009) for beams with fully bonded layers. The procedure is briefly recalled below and it will be extended later to plates with imperfect interfaces to describe layered structures with thin compliant interlayers.

3.2.1 Fully bonded layers

A continuity condition is first applied on the shear traction vectors acting at the upper and lower surfaces of the layer k and $k+1$ which are related to the shear stresses in Eq. (10). This implies equating only the part of the traction vectors which is related to the first term of the shear stresses in Eq. (8) and yields

$$
{}^{(k+1)}C_{44}(1 + {}^{(k+1)}\beta) = {}^{(k)}C_{44}(1 + {}^{(k)}\beta). \tag{11}
$$

Imposing the same condition at each interface shows that

$$
{}^{(k)}C_{44}(1 + {}^{(k)}\beta) = G, \tag{12}
$$

for $k = 1, \ldots, n-1$, with G a constant, which describes the homogenized shear rigidity of the plate. The constant G is derived by imposing a continuity condition on the longitudinal displacement at the layer interfaces, namely, ${}^{(k+1)}v_2(x_3^k) = {}^{(k)}v_2(x_3^k)$ for $k = 1, \ldots, n-1$. This and Eq. (9) yield ${}^{(k+1)}\phi(x_3^k) = {}^{(k)}\phi(x_3^k)$. Since ${}^{(k)}\beta^{(k)}h = {}^{(k)}\phi(x_3^k) - {}^{(k)}\phi(x_3^{k-1})$, from Eq. (5), integration on both sides over the thickness yields $\sum_{k=1}^{n} {}^{(k)}\beta^{(k)}h = {}^{(n)}\phi(x_3^n) - {}^{(1)}\phi(x_3^0) = 0$ and, by substituting ${}^{(k)}\beta = G/{}^{(k)}C_{44} - 1$, after Eq. (12):

$$
G = \frac{h}{\sum_{i=1}^{n} \frac{{}^{(i)}h}{{}^{(i)}C_{44}}}. \tag{13}
$$

The remaining local unknowns in the displacement field of Eq. (4), ${}^{(k)}\phi(x_3^{k-1})$ for $k = 2, \ldots, n-1$, are obtained using the relations ${}^{(k)}\phi(x_3^k) - {}^{(k)}\phi(x_3^{k-1}) = {}^{(k)}\beta^{(k)}h$ and ${}^{(k+1)}\phi(x_3^k) = {}^{(k)}\phi(x_3^k)$. This yields the recursive formula, ${}^{(k+1)}\phi(x_3^k) = {}^{(k)}\beta^{(k)}h + {}^{(k)}\phi(x_3^{k-1})$, which relates the value of the zigzag function on the lower surface of the layer $k+1$ to that on the lower surface of the layer k. Using the recursive formula to relate ${}^{(k+1)}\phi(x_3^k)$ to ${}^{(1)}\phi(x_3^0) = 0$ yields

$$
{}^{(k)}\phi(x_3^{k-1}) = \sum_{i=1}^{k-1} [{}^{(i)}\beta^{(i)}h], \tag{14}
$$

for $k = 2, \ldots, n$, and the enrichment function in a plate with perfectly bonded layers is

$$
\begin{aligned}
{}^{(k)}\phi(x_3) = &\left(\frac{G}{{}^{(k)}C_{44}} - 1\right)(x_3 - x_3^{k-1}) \\
&+ \sum_{i=1}^{k-1}\left[\left(\frac{G}{{}^{(i)}C_{44}} - 1\right){}^{(i)}h\right].
\end{aligned} \tag{15}
$$

3.2.2 Layers with imperfect interfaces

To describe plates with imperfect interfaces, the method described above is applied to a plate, where $n-1$ thin elas-

Journal: 41939 MS: 0032 TYPESET DISK LE CP Disp.:2018/8/24 Pages: 21 Layout: Large

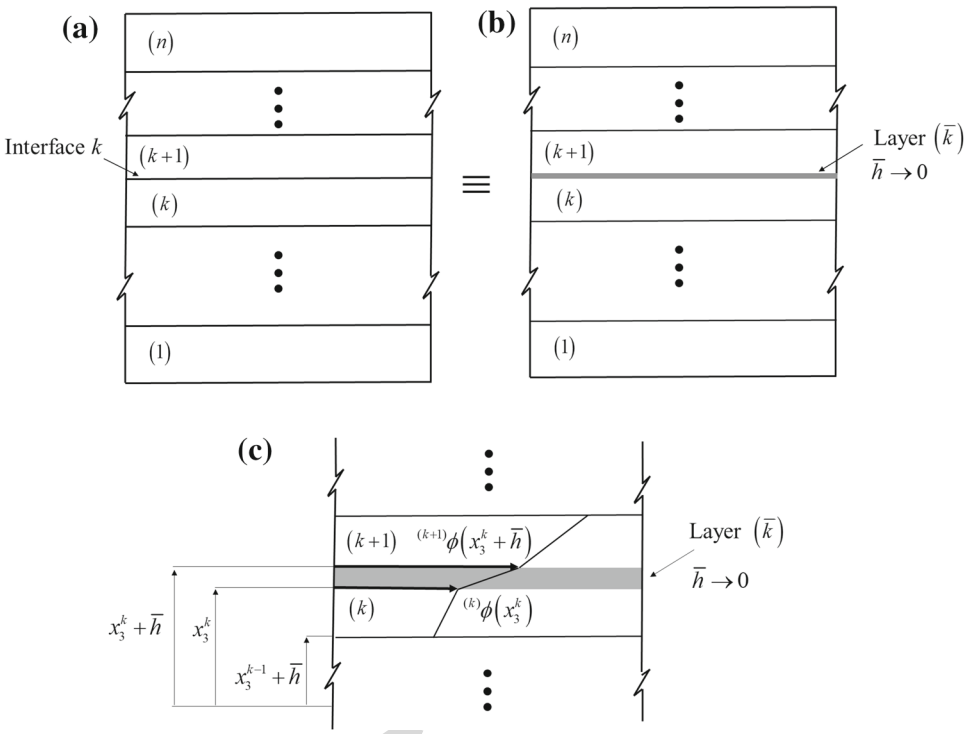

Fig. 3 **a** Layers joined by zero-thickness imperfect interfaces. **b** Layers joined by thin interlayers. **c** Zoom of the interlayer $\bar{k}$ with schematic of the zigzag function

tic interlayers $\bar{k}$ of thickness $\bar{h}$ are introduced between the regular layers of the model, Fig. 3b; the thickness of the interlayers will then be made to vanish, $\bar{h} \to 0$, to describe the plate with imperfect interfaces in Fig. 3a. The plate in Fig. 3b has $2n-1$ fully bonded layers, n regular layers and $n-1$ thin interlayers, and thickness $h+(n-1)\bar{h}$. The lower and upper surfaces of the layer k for $k=2, \ldots n$, are at the coordinates $x_3^{k-1}+\bar{h}$ and x_3^k.

The constant G in Eq. (13) modifies as

$$\bar{G} = \frac{h+(n-1)\bar{h}}{\sum_{i=1}^{n} \frac{^{(i)}h}{^{(i)}C_{44}} + \sum_{\bar{i}=1}^{n-1} \frac{\bar{h}}{^{(\bar{i})}C_{44}}}, \tag{16}$$

and the slopes of the enrichment functions in the layer and interlayer, k and $\bar{k}$, are (Fig. 3c)

$$^{(k)}\beta = \frac{\bar{G}}{^{(k)}C_{44}} - 1, \qquad ^{(\bar{k})}\beta = \frac{\bar{G}}{^{(\bar{k})}C_{44}} - 1, \tag{17}$$

where the superscript $(\bar{\bullet})$ on a quantity is used to show association with the interlayer. The imposition of the continuity condition on the longitudinal displacements at the interface between the regular layer k and the interlayer $\bar{k}-1$, $^{(k)}v_2(x_3^{k-1}+\bar{h}) = {}^{(\bar{k}-1)}v_2(x_3^{k-1}+\bar{h})$, modifies the enrichment function in Eq. (14) as

$$^{(k)}\phi(x_3^{k-1}+\bar{h}) = \sum_{i=1}^{k-1} {}^{(i)}\beta^{(i)}h + \sum_{\bar{i}=1}^{k-1} {}^{(\bar{i})}\beta\bar{h}. \tag{18}$$

In the limit for $\bar{h} \to 0$, the thin interlayer can be used to describe the zero-thickness interface, Eq. (3), by imposing that $^{(k)}\hat{v}_2 = {}^{(\bar{k})}v_2(x_3^k+\bar{h}) - {}^{(\bar{k})}v_2(x_3^k)$ and $K_S^k = {}^{(\bar{k})}C_{44}/\bar{h}$. The constant $\bar{G}$ in Eq. (16), then modifies in

$$G = \lim_{\bar{h}\to 0} \bar{G} = \frac{h}{\sum_{i=1}^{n} \frac{^{(i)}h}{^{(i)}C_{44}} + \sum_{i=1}^{n-1} \frac{1}{K_S^i}}. \tag{19}$$

If the interfaces are very stiff and $1/K_S^i = 0$, Eq. (19) describes a plate with fully bonded layers and coincides with Eq. (13). In plates with $m=1, \ldots, n-1$ debonded interfaces, $K_S^i = K_S \to 0$, $G \to 0$, and $G/K_S \to h/m$.

The slope of the enrichment function in the layer k, $^{(k)}\beta$, is obtained by substituting G, Eq. (19), into Eq. (17):

$$^{(k)}\beta = \frac{h}{^{(k)}C_{44}\left(\sum_{i=1}^{n} \frac{^{(i)}h}{^{(i)}C_{44}} + \sum_{i=1}^{n-1} \frac{1}{K_S^i}\right)} - 1, \tag{20}$$

which coincides with Eq. (12) when $1/K_S^i = 0$. In plates, where at least one of the interfaces is fully debonded and $K_S^i \to 0$, $^{(k)}\beta = -1$. In plates made of layers having the

Journal: 41939 MS: 0032 TYPESET DISK LE CP Disp.:2018/8/24 Pages: 21 Layout: Large

same elastic constants, ${}^{(k)}\beta = h/\left(h + {}^{(k)}C_{44}\sum_{i=1}^{n-1} 1/K_S^i\right) - 1$, which yields ${}^{(k)}\beta = 0$ if the layers are fully bonded.

The remaining local unknowns are derived by substituting ${}^{(\bar{k})}\beta$ from Eq. (17) into Eq. (18) and taking the limit as $\bar{h} \to 0$. This yields

$$ {}^{(k)}\phi(x_3^{k-1}) = \sum_{i=1}^{k-1}\left[\left(\frac{G}{{}^{(i)}C_{44}} - 1\right)^{(i)}h + \frac{G}{K_S^i}\right]. \tag{21} $$

Using Eqs. (17) and (21), the enrichment function, Eq. (5), becomes

$$ {}^{(k)}\phi(x_3) = \left(\frac{G}{{}^{(k)}C_{44}} - 1\right)(x_3 - x_3^{k-1}) + \sum_{i=1}^{k-1}\left[\left(\frac{G}{{}^{(i)}C_{44}} - 1\right)^{(i)}h + \frac{G}{K_S^i}\right], \tag{22} $$

which coincide with Eq. (15) in a fully bonded plate when $1/K_S^i = 0$ (Tessler et al. 2009). The particularization of the function for a plate with fully debonded layers is given in the Appendix A, where all equations related to this important special limit are presented. The procedure presented above can be used to describe plates with uniformly distributed mechanical fasteners provided K_S^i in Eqs. (19)–(22) is a measure of the elastic shear stiffness provided by the connectors.

3.3 Displacement, strain, and stress components

Once the local function in the generic layer k has been derived, Eq. (22), the displacement field, Eq. (4), is defined in terms of the four global kinematic variables, $v_{02}(x_2)$, $\varphi_2(x_2)$, $w_0(x_2)$, and $\theta_2(x_2)$ by

$$ \begin{aligned} {}^{(k)}v_2(x_2, x_3) = v_{02}(x_2) &+ \left[\varphi_2(x_2) + \theta_{2,2}(x_2)\left(\frac{G}{{}^{(k)}C_{44}} - 1\right)\right]x_3 \\ &+ \theta_{2,2}(x_2)\left(\sum_{i=1}^{k-1}\left[\left(\frac{G}{{}^{(i)}C_{44}} - 1\right)^{(i)}h + \frac{G}{K_S^i}\right]\right. \\ &\left. - \left(\frac{G}{{}^{(k)}C_{44}} - 1\right)x_3^{k-1}\right) \end{aligned} $$

$$ {}^{(k)}v_3(x_2) = w_0(x_2). \tag{23} $$

The strain and stress components in the layer k are derived from Eqs. (6) to (7):

$$ \begin{aligned} {}^{(k)}\varepsilon_{22}(x_2, x_3) = {} & v_{02,2}(x_2) \\ &+ \left[\varphi_{2,2}(x_2) + \theta_{2,2}(x_2)\left(\frac{G}{{}^{(k)}C_{44}} - 1\right)\right]x_3 \\ &+ \theta_{2,2}(x_2)\left(\sum_{i=1}^{k-1}\left[\left(\frac{G}{{}^{(i)}C_{44}} - 1\right)^{(i)}h + \frac{G}{K_S^i}\right]\right. \\ &\left. - \left(\frac{G}{{}^{(k)}C_{44}} - 1\right)x_3^{k-1}\right) \end{aligned} $$

$$ 2\,{}^{(k)}\varepsilon_{23}(x_2, x_3) = \varphi_2(x_2) + w_{0,2}(x_2) + \theta_2(x_2)\left(\frac{G}{{}^{(k)}C_{44}} - 1\right), \tag{24} $$

$$ \begin{aligned} {}^{(k)}\sigma_{22}(x_2, x_3) = {} & {}^{(k)}\bar{C}_{22}\left\{v_{02,2}(x_2) + \left[\varphi_{2,2}(x_2) + \theta_{2,2}(x_2)\right.\right. \\ &\left.\left(\frac{G}{{}^{(k)}C_{44}} - 1\right)\right]x_3 \\ &+ \theta_{2,2}(x_2)\left(\sum_{i=1}^{k-1}\left[\left(\frac{G}{{}^{(i)}C_{44}} - 1\right)^{(i)}h + \frac{G}{K_S^i}\right]\right. \\ &\left.\left. - \left(\frac{G}{{}^{(k)}C_{44}} - 1\right)x_3^{k-1}\right)\right\}{}^{(k)}\sigma_{23}(x_2, x_3) \\ = {} & {}^{(k)}C_{44}\left[\varphi_2(x_2) + w_{0,2}(x_2) + \theta_2(x_2)\left(\frac{G}{{}^{(k)}C_{44}} - 1\right)\right]. \end{aligned} \tag{25} $$

The through the thickness piecewise constant transverse shear stresses in Eq. (25) are an approximation of the actual field as a consequence of the first-order theory used to describe the global displacement field. Accurate predictions of the transverse shear stresses can be made a posteriori from the bending stresses in Eq. (25) by imposing local equilibrium ${}^{(k)}\sigma_{22,2} + {}^{(k)}\sigma_{23,3}^{\text{post}} = 0$. The interfacial jump and tractions at the interface k, Eqs. (3) and (9), become

$$ \hat{v}_2^k = \frac{G}{K_S^k}\theta_2(x_2), \tag{26} $$

$$ \hat{\sigma}_S^k = G\theta_2(x_2), \tag{27} $$

which show that, as for the shear stresses, the interfacial tractions derived through compatibility are the same for each interface of the system at a fixed coordinate x_2. Correct prediction of the interfacial tractions can be made a posteriori by imposing local equilibrium.

Displacement, strain, and stress fields in a plate with fully debonded layers are given in the Appendix A, Eqs. (45) and (46).

Journal: 41939 MS: 0032 TYPESET DISK LE CP Disp.:2018/8/24 Pages: 21 Layout: Large

3.4 Equilibrium equations and boundary conditions

The homogenized equilibrium equations and boundary conditions are derived using the principle of virtual works and following the methodology in Massabò and Campi (2014) to account for the energy contribution of the imperfect interfaces:

$$\sum_{k=1}^{n}\int_S\int_{x_3^{k-1}}^{x_3^k}({}^{(k)}\sigma_{22}\delta^{(k)}\varepsilon_{22}+2{}^{(k)}\sigma_{23}\delta^{(k)}\varepsilon_{23})\mathrm{d}x_3\mathrm{d}S + \sum_{k=1}^{n-1}\int_{(k)S^+}\hat{\sigma}_S^k\delta\hat{v}_2^k\mathrm{d}S - \int_{S^+}F_i^{S^+}\delta^{(n)}v_i\mathrm{d}S-\int_{S^-}F_i^{S^-}\delta^{(1)}v_i\mathrm{d}S-\int_B F_i^B\delta v_i\mathrm{d}B=0, \tag{28}$$

with $i=2,3$ and $F_i^{S^+}$, $F_i^{S^-}$ and F_i^B the components of the external forces acting along the boundary surfaces of the plate, S^+, S^-, and B. The symbol δ is the variational operator and the virtual displacements satisfy compatibility conditions and are independent and arbitrary. The equilibrium equations and boundary conditions are derived by substituting displacement and strain components and interfacial displacement jumps from Eqs. (23), (24), and (26) into Eq. (28) and using Green's theorem whenever necessary. The resulting equilibrium equations are:

$$\begin{aligned}&\delta v_{02}: N_{22,2}+f_2=0\\&\delta\varphi_2: M_{22,2}-Q_2+f_{2m}=0\\&\delta w_0: Q_{2,2}+f_3=0\\&\delta\theta_2: M_{22,2}^{zS}-Q_2^z-\hat{\sigma}_2=0,\end{aligned} \tag{29}$$

where the force and moment resultants and loading terms are

- normal force, bending moment, and shear force:

$$(N_{22},M_{22})=\sum_{k=1}^{n}\int_{x_3^{k-1}}^{x_3^k}{}^{(k)}\sigma_{22}(1,x_3)\mathrm{d}x_3, \tag{30}$$

$$Q_2=\sum_{k=1}^{n}\int_{x_3^{k-1}}^{x_3^k}{}^{(k)}\sigma_{23}\mathrm{d}x_3, \tag{31}$$

- moment resultant and shear force associated to the enrichment field:

$$\begin{aligned}M_{22}^{zS}&=\sum_{k=1}^{n}\int_{x_3^{k-1}}^{x_3^k}{}^{(k)}\sigma_{22}\left\{\left(\frac{G}{{}^{(k)}C_{44}}-1\right)(x_3-x_3^{k-1})+\sum_{i=1}^{k-1}\left[\left(\frac{G}{{}^{(i)}C_{44}}-1\right)^{(i)}h+\frac{G}{K_S^i}\right]\right\}\mathrm{d}x_3,\\Q_2^z&=\sum_{k=1}^{n}\int_{x_3^{k-1}}^{x_3^k}{}^{(k)}\sigma_{23}\left(\frac{G}{{}^{(k)}C_{44}}-1\right)\mathrm{d}x_3,\\\hat{\sigma}_2&=G\sum_{k=1}^{n-1}\frac{\hat{\sigma}_S^k}{K_S^k}\ \text{or}\ \hat{\sigma}_2=\hat{A}_{44}^S\theta_2(x_2),\end{aligned} \tag{32}$$

with $\hat{A}_{44}^S=G^2\sum_{k=1}^{n-1}\frac{1}{K_S^k}$.

- distributed tangential and transverse forces and couples:

$$\begin{aligned}f_2&=F_2^{S+}+F_2^{S-},\\f_{2m}&=F_2^{S+}x_3^n+F_2^{S-}x_3^0,\\f_3&=F_3^{S+}+F_3^{S-}.\end{aligned} \tag{33}$$

The form of the first three equilibrium equations in Eq. (29) is analogous to that of the first-order shear deformation theory, but the force and moment resultants differ, since they account for the effects of the local enrichment through the stresses, Eq. (25). The fourth equilibrium equation is needed to define the additional global variable.

The boundary conditions at the plate edges, $x_2=0,\ L$, with $n=\{0,\pm1,0\}^{\mathrm{T}}$ the outward normal, are

$$\begin{aligned}&\delta v_{02}: N_{22}n_2=\tilde{N}_2\quad\text{or}\quad v_{02}=\tilde{v}_{02}\\&\delta\varphi_2: M_{22}n_2=\tilde{M}_2\quad\text{or}\quad\varphi_2=\tilde{\varphi}_2\\&\delta w_0: Q_2n_2=\tilde{Q}_2\quad\text{or}\quad w_0=\tilde{w}_0\\&\delta\theta_2: M_{22}^{zS}n_2=\tilde{M}_2^{zS}\quad\text{or}\quad\theta_2=\tilde{\theta}_2,\end{aligned} \tag{34}$$

where the terms with the tilde define prescribed values of displacements, forces and couples:

$$\begin{aligned}(\tilde{N}_2,\tilde{Q}_2)&=\sum_{k=1}^{n}\int_{x_3^{k-1}}^{x_3^k}({}^{(k)}F_2^B,{}^{(k)}F_3^B)\mathrm{d}x_3,\\\tilde{M}_2&=\sum_{k=1}^{n}\int_{x_3^{k-1}}^{x_3^k}{}^{(k)}F_2^Bx_3\mathrm{d}x_3,\\\tilde{M}_2^{zS}&=\sum_{k=1}^{n}\int_{x_3^{k-1}}^{x_3^k}{}^{(k)}F_2^B\left\{\left(\frac{G}{{}^{(k)}C_{44}}-1\right)(x_3-x_3^{k-1})+\sum_{i=1}^{k-1}\left[\left(\frac{G}{{}^{(i)}C_{44}}-1\right)^{(i)}h+\frac{G}{K_S^i}\right]\right\}\mathrm{d}x_3.\end{aligned} \tag{35}$$

Journal: 41939 MS: 0032 TYPESET DISK LE CP Disp.:2018/8/24 Pages: 21 Layout: Large

The homogenized constitutive equations of the plate are derived by substituting the stress components from Eq. (25) into the stress resultants defined in Eqs. (30)–(32):

$$\begin{Bmatrix} N_{22} \\ M_{22} \\ M_{22}^{zS} \end{Bmatrix} = \begin{bmatrix} A_{22} & B_{22} & B_{22}^{S} \\ B_{22} & D_{22} & D_{22}^{S} \\ B_{22}^{S} & D_{22}^{S} & D_{22}^{SS} \end{bmatrix} \begin{Bmatrix} v_{02,2} \\ \varphi_{2,2} \\ \theta_{2,2} \end{Bmatrix}$$
$$\begin{Bmatrix} Q_2 \\ Q_2^{z} \end{Bmatrix} = k_{44} \begin{bmatrix} A_{44} & A_{44}^{S} \\ A_{44}^{S} & A_{44}^{SS} \end{bmatrix} \begin{Bmatrix} \varphi_2 + w_{0,2} \\ \theta_2 \end{Bmatrix}, \tag{36}$$

where the homogenized (effective) elastic stiffnesses of the plate are

$$[A_{22}, B_{22}, D_{22}] = \sum_{k=1}^{n} {}^{(k)}\bar{C}_{22} \int_{x_3^{k-1}}^{x_3^{k}} [1, x_3, (x_3)^2] \mathrm{d}x_3$$
$$B_{22}^{S} = \sum_{k=1}^{n} {}^{(k)}\bar{C}_{22} \int_{x_3^{k-1}}^{x_3^{k}} \left\{ \left(\frac{G}{{}^{(k)}C_{44}} - 1 \right)(x_3 - x_3^{k-1}) + \sum_{i=1}^{k-1} \left[\left(\frac{G}{{}^{(i)}C_{44}} - 1 \right)^{(i)}h + \frac{G}{K_S^i} \right] \right\} \mathrm{d}x_3$$
$$D_{22}^{S} = \sum_{k=1}^{n} {}^{(k)}\bar{C}_{22} \int_{x_3^{k-1}}^{x_3^{k}} x_3 \left\{ \left(\frac{G}{{}^{(k)}C_{44}} - 1 \right)(x_3 - x_3^{k-1}) + \sum_{i=1}^{k-1} \left[\left(\frac{G}{{}^{(i)}C_{44}} - 1 \right)^{(i)}h + \frac{G}{K_S^i} \right] \right\} \mathrm{d}x_3$$
$$D_{22}^{SS} = \sum_{k=1}^{n} {}^{(k)}\bar{C}_{22} \int_{x_3^{k-1}}^{x_3^{k}} \left\{ \left(\frac{G}{{}^{(k)}C_{44}} - 1 \right)(x_3 - x_3^{k-1}) + \sum_{i=1}^{k-1} \left[\left(\frac{G}{{}^{(i)}C_{44}} - 1 \right)^{(i)}h + \frac{G}{K_S^i} \right] \right\}^2 \mathrm{d}x_3$$
$$[A_{44}, A_{44}^{S}, A_{44}^{SS}] = \sum_{k=1}^{n} {}^{(k)}C_{44}{}^{(k)}h \times \left[1, \frac{G}{{}^{(k)}C_{44}} - 1, \left(\frac{G}{{}^{(k)}C_{44}} - 1 \right)^2 \right]$$
$$\hat{A}_{44}^{S} = G^2 \sum_{k=1}^{n-1} \frac{1}{K_S^k}. \tag{37}$$

A shear correction factor, k_{44}, has been introduced in Eq. (36) to improve the approximate description of the shear strains of the model. In the limiting case of a fully bonded and homogeneous plate, the zigzag enrichment is zero and the model proposed here coincides with first-order shear deformation theory, for which a shear correction factor is required to match elasticity solutions. As demonstrated in Massabò (2017), for the dynamic correction factor of the homogenized structural model in Massabò and Campi (2014), the results in Sect. 4 will show that the correction factor obtained for a fully bonded homogeneous material can be applied also to layered materials and in the presence of imperfect interfaces.

Substitution of the force and moment resultants from Eq. (36) into Eqs. (29) and (34) yields the equilibrium equations in terms of global displacements:

$$\begin{aligned}
&\delta v_{02} : A_{22} v_{02,22} + B_{22}\varphi_{2,22} + B_{22}^{S}\theta_{2,22} + f_2 = 0 \\
&\delta \varphi_2 : B_{22} v_{02,22} + D_{22}\varphi_{2,22} + D_{22}^{S}\theta_{2,22} \\
&\quad - k_{44}A_{44}(\varphi_2 + w_{0,2}) - k_{44}A_{44}^{S}\theta_2 + f_{2m} = 0 \\
&\delta w_0 : k_{44}A_{44}(\varphi_{2,2} + w_{02,22}) + k_{44}A_{44}^{S}\theta_{2,2} + f_3 = 0 \\
&\delta \theta_2 : B_{22}^{S} v_{02,22} + D_{22}^{S}\varphi_{2,22} + D_{22}^{SS}\theta_{2,22} \\
&\quad - k_{44}A_{44}^{S}(\varphi_2 + w_{0,2}) - (k_{44}A_{44}^{SS} + \hat{A}_{44}^{S})\theta_2 = 0,
\end{aligned} \tag{38}$$

and the boundary conditions:

$$\begin{aligned}
&\delta v_{02} : (A_{22}v_{02,2} + B_{22}\varphi_{2,2} + B_{22}^{S}\theta_{2,2})n_2 = \tilde{N}_2 \quad \text{or} \quad v_{02} = \tilde{v}_{02} \\
&\delta \varphi_2 : (B_{22}v_{02,2} + D_{22}\varphi_{2,2} + D_{22}^{S}\theta_{2,2})n_2 = \tilde{M}_2 \quad \text{or} \quad \varphi_2 = \tilde{\varphi}_2 \\
&\delta w_0 : k_{44}(A_{44}(\varphi_2 + w_{0,2}) + A_{44}^{S}\theta_2)n_2 = \tilde{Q}_3 \quad \text{or} \quad w_0 = \tilde{w}_0 \\
&\delta \theta_2 : (B_{22}^{S}v_{02,2} + D_{22}^{S}\varphi_{2,2} + D_{22}^{SS}\theta_{2,2})n_2 = \tilde{M}_2^{zS} \quad \text{or} \quad \theta_2 = \tilde{\theta}_2.
\end{aligned} \tag{39}$$

The governing field equations (38) and (39) have order VIII. They are decoupled for efficient closed-form solution in Appendix B.

In a plate, where the interfaces are fully bonded, the equilibrium equations are obtained by setting $1/K_S^i = 0$ in the coefficients in Eq. (37); this yields $\hat{A}_{44}^{S} = 0$. If in addition the plate is composed of layers having the same material properties, e.g., a unidirectionally reinforced laminate, the coefficients with superscript S, namely, B_{22}^{S}, D_{22}^{S}, D_{22}^{SS}, A_{44}^{S}, and A_{44}^{SS}, become zero, since $G = C_{44}$. The terms of the equations multiplying θ_2 vanish and the order of the equations reduce to VI; the fourth equilibrium equation and boundary condition become identities and the model coincides with the first-order shear deformation theory:

$$\begin{aligned}
&\bar{C}_{22}h v_{02,22} = 0 \\
&w_{0,2222} + \frac{1}{k_{44}C_{44}h} f_{3,22} - \frac{1}{\frac{1}{12}\bar{C}_{22}h^3} f_3 = 0 \\
&\varphi_{2,2} = -w_{0,22} - \frac{1}{k_{44}C_{44}h} f_3,
\end{aligned} \tag{40}$$

where the classical shear correction factor is required.

In a plate made of layers having the same thickness, h/n, and elastic constants and where the interfaces are fully

Journal: 41939 MS: 0032 TYPESET DISK LE CP Disp.:2018/8/24 Pages: 21 Layout: Large

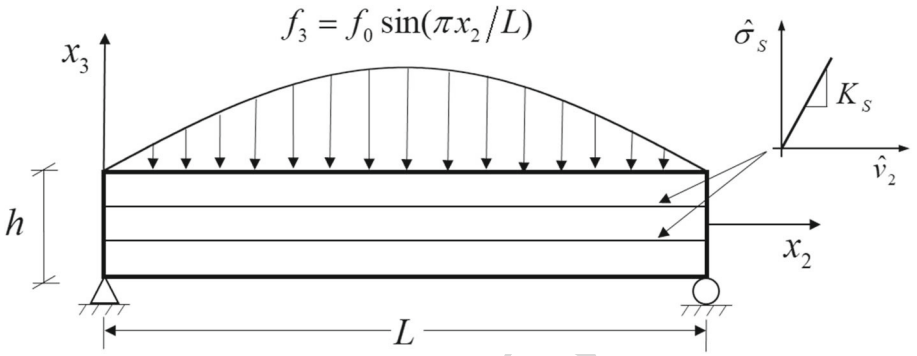

Fig. 4 Three-layer wide plate with linear-elastic interfaces subjected to sinusoidal transverse loading

debonded, Eq. (38) along with Eq. (48) in Appendix A for a coordinate system placed at the mid-thickness, yields

$$\begin{aligned}
&\bar{C}_{22}\frac{h}{n}v_{02,22} = 0\\
&w_{0,2222} + \frac{1}{k_{44}C_{44}\frac{h}{n}}\left(\frac{f_3}{n}\right)_{,22} - \frac{1}{\frac{1}{12}\bar{C}_{22}\left(\frac{h}{n}\right)^3}\left(\frac{f_3}{n}\right) = 0\\
&(\varphi_2 - \theta_2)_{,2} = -w_{0,22} - \frac{1}{k_{44}C_{44}\left(\frac{h}{n}\right)}\left(\frac{f_3}{n}\right)\\
&\theta_{2,22} = -\frac{n-1}{n}(\varphi_2 - \theta_2)_{,22}.
\end{aligned} \tag{41}$$

Comparing the first three equations in Eqs. (40) and (41) shows that the plate with fully debonded layers behaves like a stack of layers of thickness, h/n, free to slide along each other and whose behavior is described by the first-order shear deformation theory and require the use of the classical shear correction factor. The fourth equation in (41) is used to define the variable θ_2 which provides the effects of the local field, including the jump at the interfaces, $\hat{v}_2^i = h\theta_2/(n-1)$ for $i = 1, \ldots, n-1$, Eq. (26).

4 Applications

In this section, some applications are presented to verify the accuracy of the model, through comparison with 2D elasticity solutions, and highlight improvements/limitations with respect to other structural models based on a similar homogenized approach. In all applications, the shear correction factor has been assumed as $k_{44} = 5/6$, which is the value obtained by matching the shear elastic energy of a fully bonded homogeneous plate under constant transverse shear to that of 2D elasticity (Jourawsky approximation).

4.1 Simply supported plate

The simply supported wide plate with imperfect interfaces subjected to sinusoidal transverse loading, $f_3 = f_0 \sin(\pi x_2/L)$, acting on the upper surface of the plate is considered first, Fig. 4. The plate has length-to-thickness ratio $L/h = 4$ and is made by three orthotropic layers with elastic constants $E_T/E_L = 1/25$, $G_{LT}/E_L = 1/50$, $G_{TT}/E_L = 1/125$, and $\nu_{LT} = \nu_{TT} = 0.25$, and principal material directions along the coordinate axes; the assumed ratios could represent a graphite–epoxy composite (L and T indicate directions parallel and transverse to the fibers). The layers are connected by linear-elastic interfaces with the same interfacial stiffness, K_S.

The problem is solved using the decoupled equations (40), (41), and (49) and imposing the boundary conditions (34), which particularize to

$$\begin{aligned}
&x_2 = 0 : \tilde{w}_0 = \tilde{v}_{02} = \tilde{M}_2 = \tilde{M}_2^{zS} = 0\\
&x_2 = L : \tilde{w}_0 = \tilde{N}_2 = \tilde{M}_2 = \tilde{M}_2^{zS} = 0.
\end{aligned} \tag{42}$$

The variable θ_2 is set to zero at the mid-span for the symmetry of the problem. Once the global variables $v_{02}(x_2)$, $\varphi_2(x_2)$,$w_0(x_2)$, and $\theta_2(x_2)$ are obtained, local displacements, bending stresses, interfacial tractions, and jumps are defined through Eqs. (23) and (25)–(27). The transverse shear stresses are derived from the bending stresses imposing local equilibrium. The results will be compared with the explicit 2D elasticity solutions in Darban and Massabò (2017b).

4.1.1 Unidirectionally reinforced plate with imperfect interfaces

In this application, the layers are assumed to have stacking sequence (0, 0, 0). This example allows to focus on the effects of the presence of imperfect interfaces on the local and global responses of the plate. The through-thickness variation of the longitudinal displacements at $x_2 = 0$ and the transverse displacements at $x_2 = L/2$ are shown in Fig. 5. Results for the bending stresses at $x_2 = L/2$ and transverse shear stresses at $x_2 = 0$ are shown through the thickness in Fig. 6. Three cases are analyzed: perfectly bonded interfaces, with $1/K_S = 0$, interfaces with intermediate stiffness, with $K_S h/\bar{E}_L = 0.01$, and fully debonded interfaces, with $K_S = 0$.

Journal: 41939 MS: 0032 TYPESET DISK LE CP Disp.:2018/8/24 Pages: 21 Layout: Large

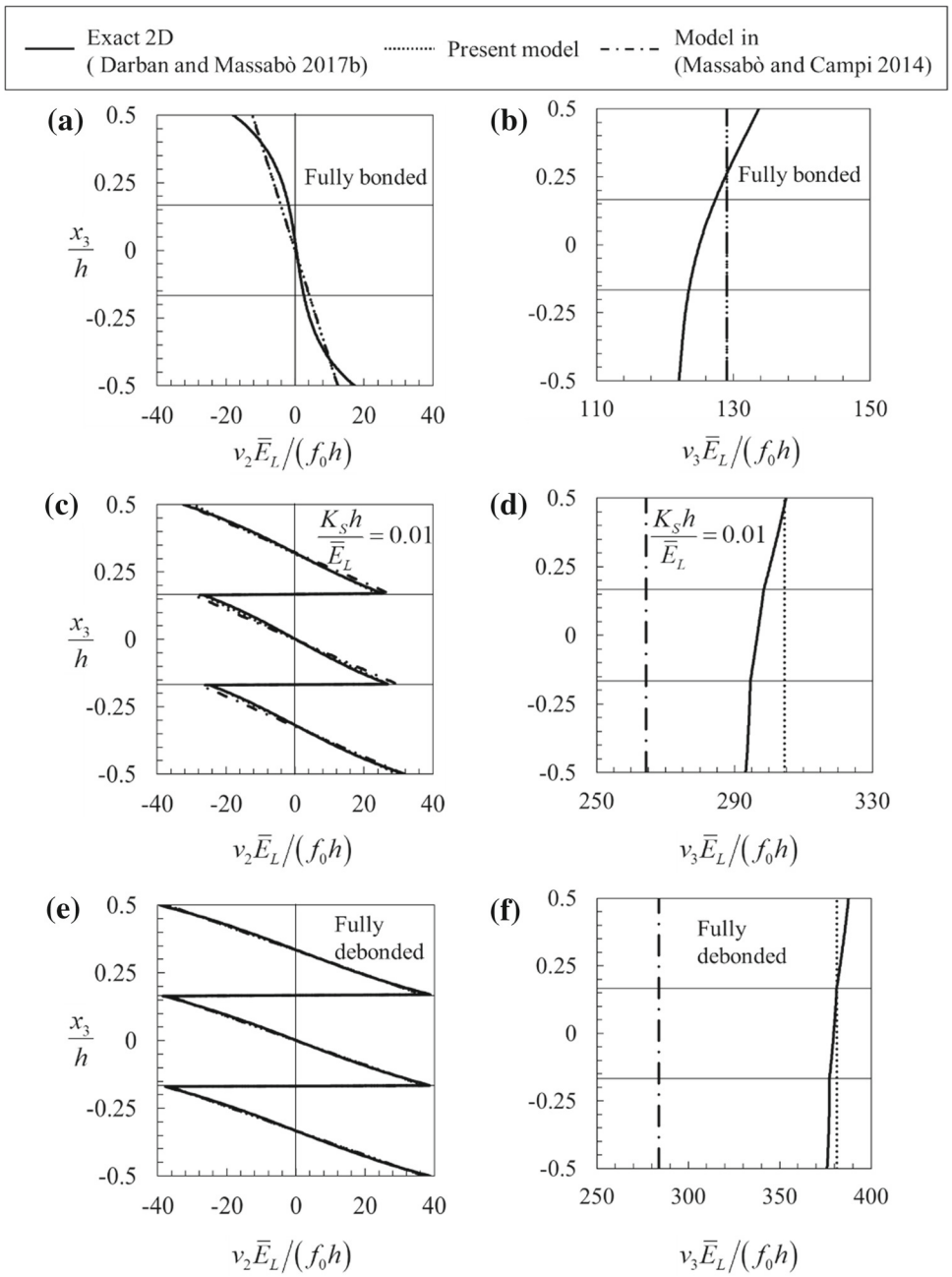

Fig. 5 Longitudinal, at $x_2 = 0$, and transverse, at $x_2 = L/2$, displacements shown through the thickness in a simply supported wide plate with $L/h = 4$, stacking sequence (0, 0, 0), transverse loading $f_3 = f_0 \sin(\pi x_2/L)$. Elastic constants: $E_T/E_L = 1/25$, $G_{LT}/E_L = 1/50$, $G_{TT}/E_L = 1/125$ and $\nu_{LT} = \nu_{TT} = 0.25$, and $\bar{E}_L = \bar{C}_{22} = E_L/(1 - \nu_{LT}\nu_{TL})$

The structural theory accurately captures the interfacial displacement jumps due to the presence of the imperfect interfaces; longitudinal displacements, bending, and transverse shear stresses are accurate for all cases examined. The transverse displacement of the fully bonded case slightly overestimates the average transverse displacement of the 2D elasticity solution due to the use of a shear correction factor which has been derived for constant transverse shear, $k_{44} = 5/6 = 0.833$. If the shear elastic energy was matched to the 2D elasticity solution (Darban and Massabò 2017b) for the loading conditions assumed in this problem, a correction factor equal to 0.936 would be obtained, which would improve predictions. The accuracy in the prediction of the transverse displacements improves on decreasing the interfacial stiffness, since the three layers progressively behave as individual thinner plates. For plates with higher length-to-thickness ratios, e.g., $L/h \geq 10$, the difference between the predictions of the model and exact solution significantly reduces for all interfacial stiffness values (not shown).

The results obtained using the homogenized model in Massabò and Campi (2014) are also shown in Figs. 5 and 6. The solutions of the two structural models virtually coincide but for the mid-span deflection when the interfaces are imperfect or fully debonded; for these cases, the model for-

Journal: 41939 MS: 0032 TYPESET DISK LE CP Disp.:2018/8/24 Pages: 21 Layout: Large

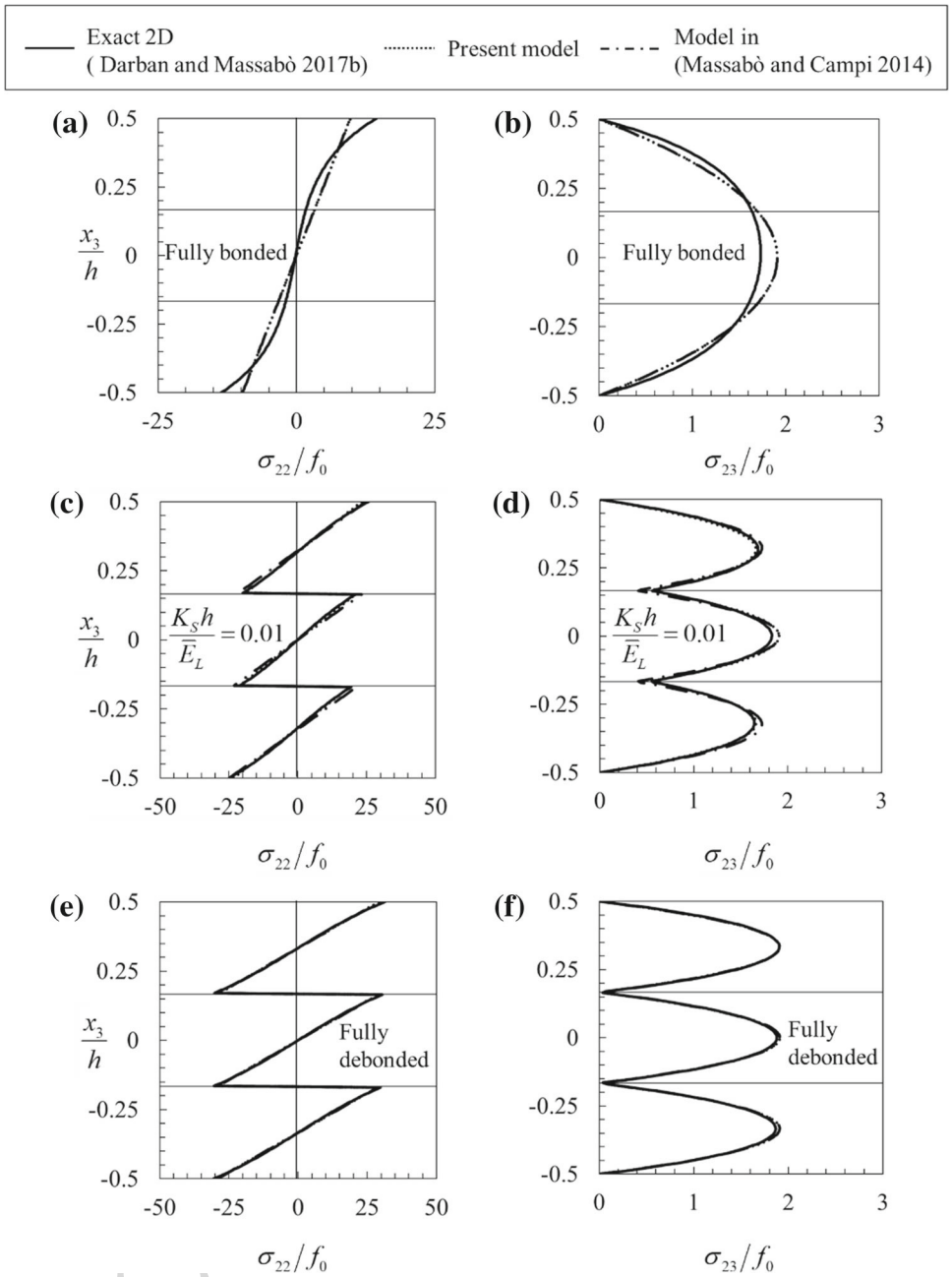

Fig. 6 Bending at $x_2 = L/2$ and transverse shear at $x_2 = 0$ stresses through the thickness in a simply supported three-layer, unidirectionally reinforced wide plate $(0, 0, 0)$, $L/h = 4$, transverse loading $f_3 = f_0 \sin(\pi x_2/L)$. Elastic constants: $E_T/E_L = 1/25$, $G_{LT}/E_L = 1/50$, $G_{TT}/E_L = 1/125$ and $\nu_{LT} = \nu_{TT} = 0.25$, and $\bar{E}_L = \bar{C}_{22} = E_L/(1 - \nu_{LT}\nu_{TL})$. Transverse shear stresses are calculated a posteriori from bending stresses

mulated here performs better due to a better description of the shear deformations. The highest improvement in the solution is for the case of fully debonded layers for which the model in Massabò and Campi (2014) fully neglects the contribution of the shear deformations to the transverse compliance as a consequence of the continuity imposed between the transverse tractions at the layer surfaces and the interfacial tractions. Solutions obtained by other models using a similar zigzag homogenization are not shown, because they are affected by energy inconsistencies which yield important inaccuracies [see discussion in Massabò and Campi (2015)].

4.1.2 Multilayered plate with imperfect interfaces

In this section, the plate in Fig. 4 is studied assuming a stacking sequence of $(0, 90, 0)$. This problem provides a challenging case to assess the predictive capabilities of the approximate model due to the highly anisotropic layup of the thick plate. The through-thickness variation of the longitudinal and transverse displacements, and bending and transverse shear stresses at different cross sections of the plate are shown in Figs. 7 and 8. Results are presented on varying the interfacial stiffness.

Journal: 41939 MS: 0032 TYPESET DISK LE CP Disp.:2018/8/24 Pages: 21 Layout: Large

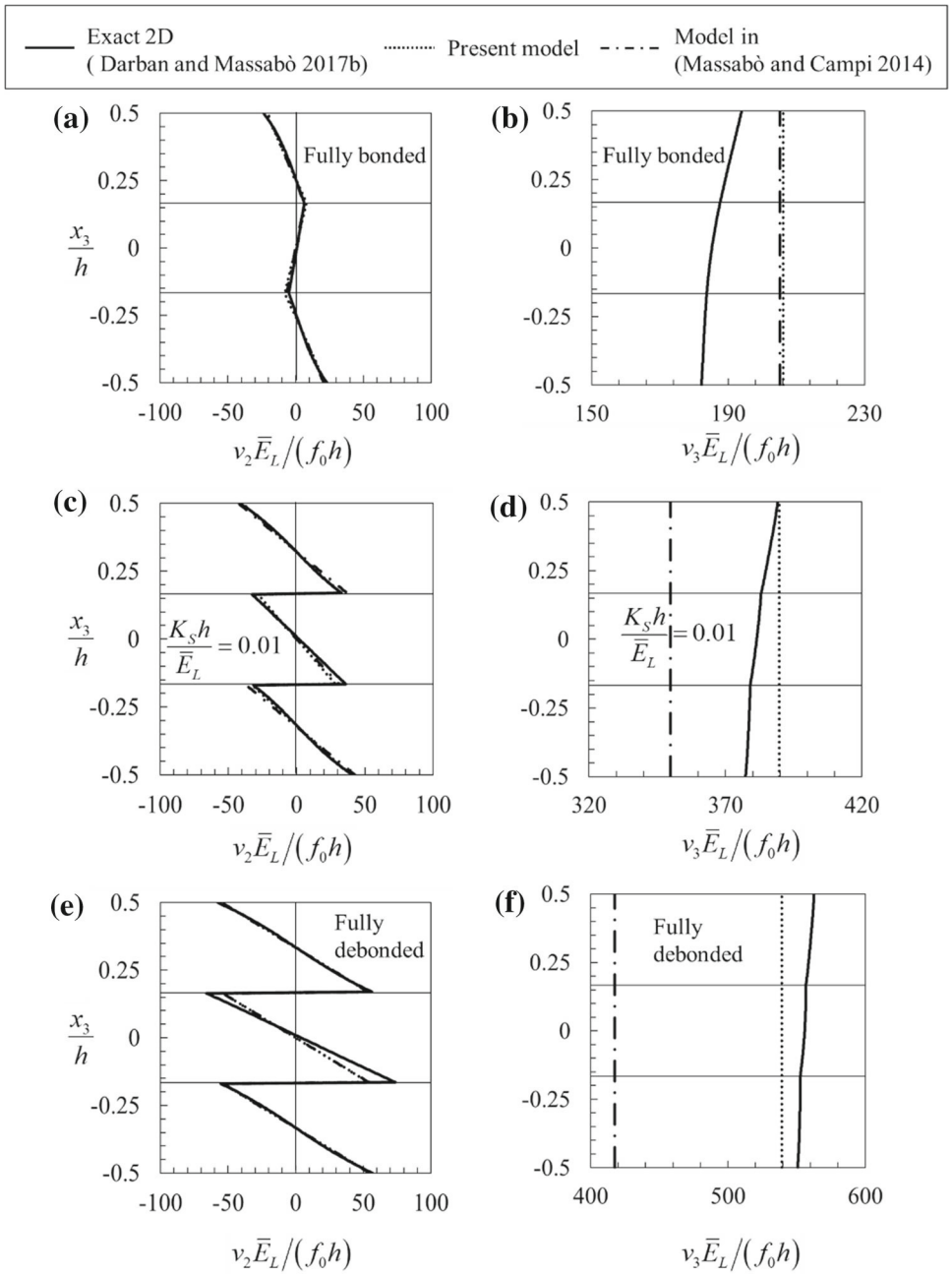

Fig. 7 Longitudinal at $x_2 = 0$ and transverse at $x_2 = L/2$ displacements through the thickness in a simply supported three-layer wide plate (0, 90, 0), $L/h = 4$, transverse loading $f_3 = f_0 \sin(\pi x_2/L)$. Elastic constants: $E_T/E_L = 1/25$, $G_{LT}/E_L = 1/50$, $G_{TT}/E_L = 1/125$ and $\nu_{LT} = \nu_{TT} = 0.25$, and $\bar{E}_L = \bar{C}_{22} = E_L/(1 - \nu_{LT}\nu_{TL})$

The structural model well captures the zigzag patterns in the longitudinal displacements of the layers and the interfacial displacement jumps. The bending and transverse shear stresses are also in good agreement with the exact 2D elasticity solutions. The transverse displacement of the fully bonded case overestimates the average transverse displacement of the 2D elasticity solution and the relative error is around 11%. The predictions improve on reducing the interfacial stiffness up to the fully debonded case, since the behavior is then controlled by the response of three separate thinner layers, and the relative error reduces to 3%. Using the correction factor derived by matching the 2D elasticity shear strain energy for this loading case in a homogeneous material, $k_{44} = 0.936$, instead of the value 5/6 obtained assuming constant shear would improve the solutions in all cases and reduce the error. These results confirm what already found for the dynamic correction factor in Massabò (2017): no changes in the correction factor are needed in the homogenized structural model to account for the multilayered structure, which is already described through the multiscale treatment and the zigzag enrichment.

As already noted for the previous example, the present model predicts the transverse displacements more accurately than the model in Massabò and Campi (2014). For plates

Journal: 41939 MS: 0032 TYPESET DISK LE CP Disp.:2018/8/24 Pages: 21 Layout: Large

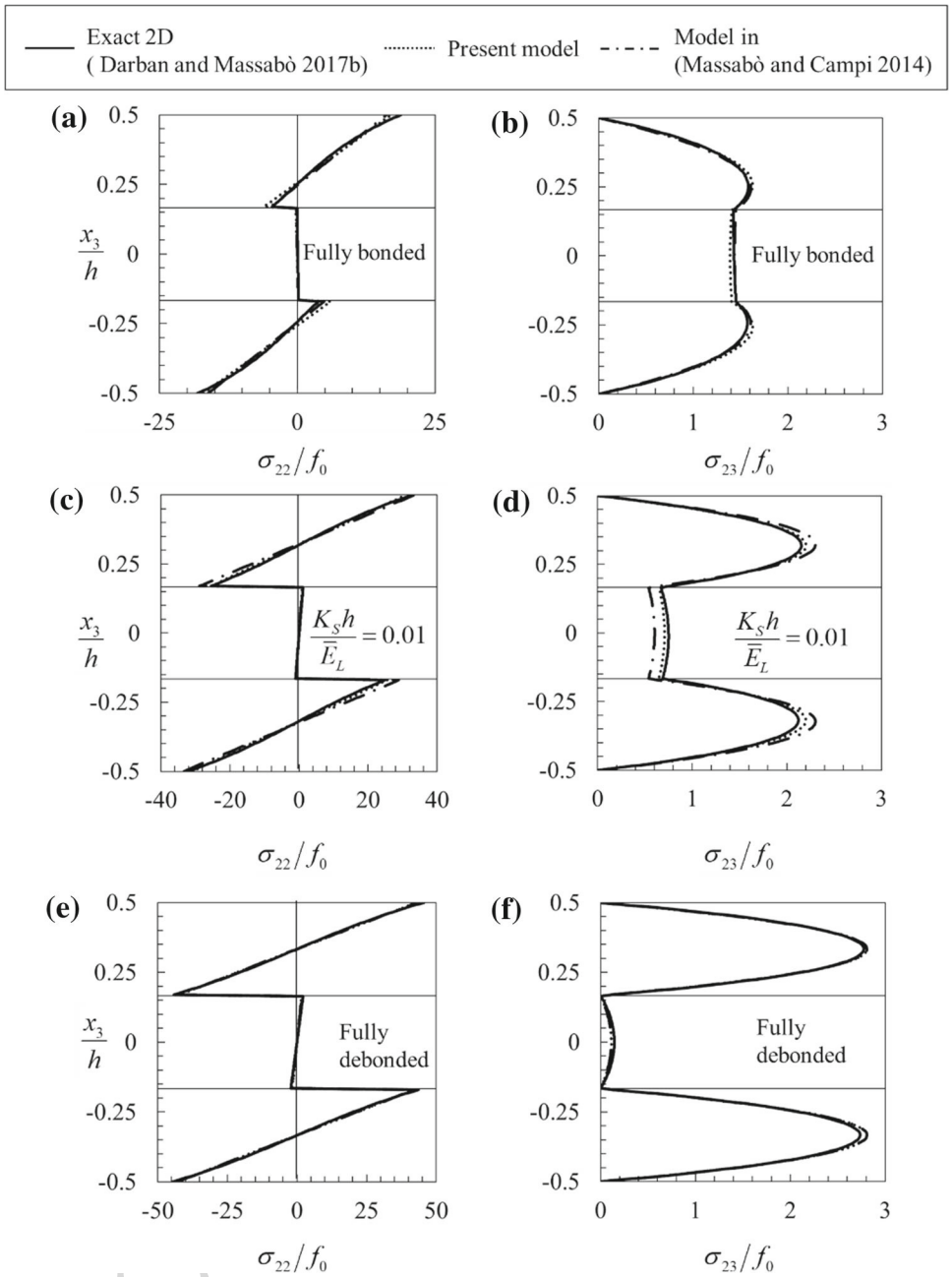

Fig. 8 Bending at $x_2 = L/2$ and transverse shear at $x_2 = 0$ stresses through the thickness in a simply supported three-layer wide plate (0, 90, 0), $L/h = 4$, transverse loading $f_3 = f_0 \sin(\pi x_2/L)$. Elastic constants: $E_T/E_L = 1/25$, $G_{LT}/E_L = 1/50$, $G_{TT}/E_L = 1/125$ and $\nu_{LT} = \nu_{TT} = 0.25$, and $\bar{E}_L = \bar{C}_{22} = E_L/(1 - \nu_{LT}\nu_{TL})$. Transverse shear stresses are calculated a posteriori from bending stresses

with higher length-to-thickness ratios, e.g., $L/h \geq 10$, the solution significantly improves and the difference between the predictions of the models and the exact solutions significantly reduces for all interfacial stiffness values (not shown).

To further illustrate the capability of the homogenized model to predict the transverse displacements also in plates with imperfect interfaces, the mid-span displacement is shown on varying the interfacial stiffness (decreasing interfacial stiffness from left to right) in Fig. 9. The displacement is normalized to the thickness average 2D elasticity solution of a fully debonded plate, $(v_3)_{2D,\text{lim}}$.

Predictions using the homogenized model in Massabò and Campi (2014) are also shown in Fig. 9 [solutions based on other homogenized approaches are not presented because of the energy inconsistencies discussed in Massabò and Campi (2015)]. As already explained in Massabò and Campi (2014) for a homogeneous material, this result is a consequence of the imposition of continuity conditions on the transverse shear tractions and the interfacial tractions. In thick plates with imperfect or fully debonded interfaces, this leads to an important underestimation of the shear contribution to the transverse compliance.

Journal: 41939 MS: 0032 TYPESET DISK LE CP Disp.:2018/8/24 Pages: 21 Layout: Large

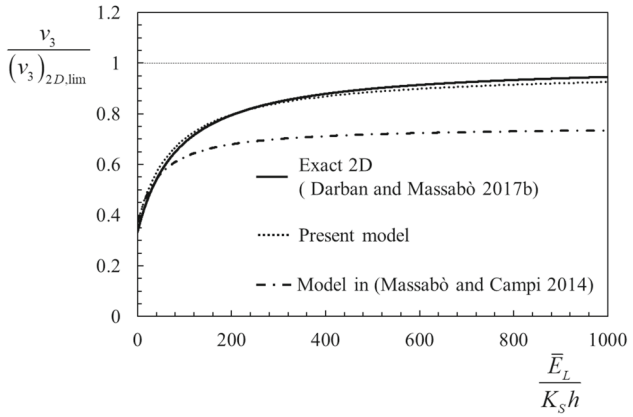

Fig. 9 Mid-thickness transverse displacements at $x_2 = L/2$ of a simply supported three-layer, unidirectionally reinforced wide plate (0, 90, 0), $L/h = 4$, transverse loading $f_3 = f_0 \sin(\pi x_2/L)$; $(v_3)_{2D,\lim}$ is the thickness average 2D elasticity solution of a fully debonded plate. Elastic constants: $E_T/E_L = 1/25$, $G_{LT}/E_L = 1/50$, $G_{TT}/E_L = 1/125$ and $\nu_{LT} = \nu_{TT} = 0.25$, and $\bar{E}_L = \bar{C}_{22} = E_L/(1 - \nu_{LT}\nu_{TL})$

4.2 Cantilevered wide plate

To verify the predictive capabilities of the model in problems with clamped edges, the cantilevered wide plate with $L/h = 10$ and two equal thickness layers connected by a linear-elastic interface is examined. The plate is subjected to a concentrated transverse force at the free end, Fig. 10. The elastic constants are $E_T/E_L = 1/25$, $G_{LT}/E_L = 1/50$, $G_{TT}/E_L = 1/125$ and $\nu_{LT} = \nu_{TT} = 0.25$. Two stacking sequences are examined: (0, 0) and (90, 0) with the 0° layer being the upper one. The boundary conditions are

$$x_2 = 0 : \tilde{w}_0 = \tilde{v}_{02} = \tilde{\varphi}_2 = \tilde{\theta}_2 = 0$$
$$x_2 = L : \begin{cases} \tilde{N}_2 = \tilde{M}_2 = \tilde{M}_2^{zS} = 0 \\ \tilde{Q}_2 = -F \end{cases} . \tag{43}$$

Figure 11a depicts the interfacial shear tractions, $\hat{\sigma}_S$, Eq. (27), along the plate length for four values of the interfacial stiffness in the plate with the (0, 0) stacking sequence; the interfacial tractions coincide with those calculated a posteriori from local equilibrium. The results are compared with those of a discrete layer interface model (Andrews et al. 2009) which represents the two layers as individual plates connected by interfacial normal and tangential tractions. The interfacial shear tractions predicted by the model proposed here coincide with those obtained by the discrete layer model for any values of the interfacial stiffness. Results obtained using the model in Massabò and Campi (2014) are also shown in Fig. 11a and highlight some inaccuracies for the intermediate values of interfacial stiffness.

Figure 11b depicts interfacial tractions calculated a posteriori from local equilibrium in the plate with (90, 0) layup. As for the previous case, the interfacial tractions are in agreement with those of the discrete layer model for very large and very small values of the interfacial stiffness over the entire length of the plate except at the clamped boundary, where the tractions predicted by the present model do not vanish at the support. Some differences are observed for intermediate values of the interfacial stiffnesses which are due to the assumption of neglecting the interfacial normal tractions in the solution of the problem. A similar discrepancy would be observed in all problems, where the interfacial normal tractions are nonzero due to the lack of symmetry, e.g., in a specimen with (0, 0) layup and unequal thickness layers. The results would improve by accounting for the interfacial normal tractions following, for instance, the methodology in Massabò and Campi (2014). The results have not been compared with 2D solutions and inaccuracies in the predictions, similar to those observed in Groh and Tessler (2017) for fully bonded plates, are expected at the clamped edge due to the limitations of the structural theory.

4.3 Plate with in-plane material discontinuity

The proposed model shows some limitations when applied to study plates with in-plane discontinuities, due to changes in the material properties of the layers or to the presence of regions, where the status of the interfaces changes. This behavior is controlled by the parameter G, which defines the homogenized shear rigidity of the different domains of the plate, Eq. (19). When the difference in G between two continuous domains is small the results are quite accurate, while for large differences, important inaccuracies are observed.

To illustrate this behavior the End Notched Flexural specimen in Fig. 12a, with normalized length $2L/h = 100$ and crack length $a/h = 30$ has been analyzed. The material is homogeneous and the elastic constants are $E_T/E_L = 1/25$, $G_{LT}/E_L = 1/50$, $G_{TT}/E_L = 1/125$, and $\nu_{LT} = \nu_{TT} = 0.25$. The crack is described by introducing at mid-thickness and for $0 \le x_2 \le a$ an imperfect interface with a very small interfacial stiffness, $K_S h/\bar{E}_L = 10^{-4}$, with $\bar{E}_L = \bar{C}_{22} = E_L/(1 - \nu_{LT}\nu_{TL})$; this implies that the normalized value of the homogenized shear rigidity in the delaminated region is $G/G_{LT} = 0.01$. The fully bonded region, for $a \le x_2 \le 2L$, is described by inserting a mid-thickness interface with interfacial stiffness $K_S h/\bar{E}_L = 10^4$, which implies a homogenized shear rigidity $G/G_{LT} = 0.99$. The boundary conditions at $x_2 = 0$ and $x_2 = 2L$ are those given in Eq. (42), and the continuity conditions at $x_2 = a$ and $x_2 = L$ are imposed on the global variables and force and moment resultants.

The deformed shape of the specimen is shown in Fig. 12b. The results are compared with those predicted by a discrete layer interface model and show an unrealistic discontinuity in the slope of the curve at the crack tip cross section. For

Journal: 41939 MS: 0032 TYPESET DISK LE CP Disp.:2018/8/24 Pages: 21 Layout: Large

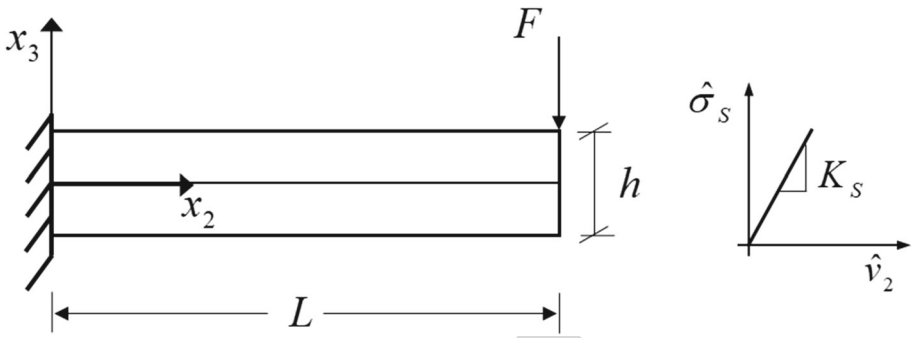

Fig. 10 Cantilevered plate composed of two equal thickness layers joined by a linear-elastic interface and subjected to a transverse load F at the free end

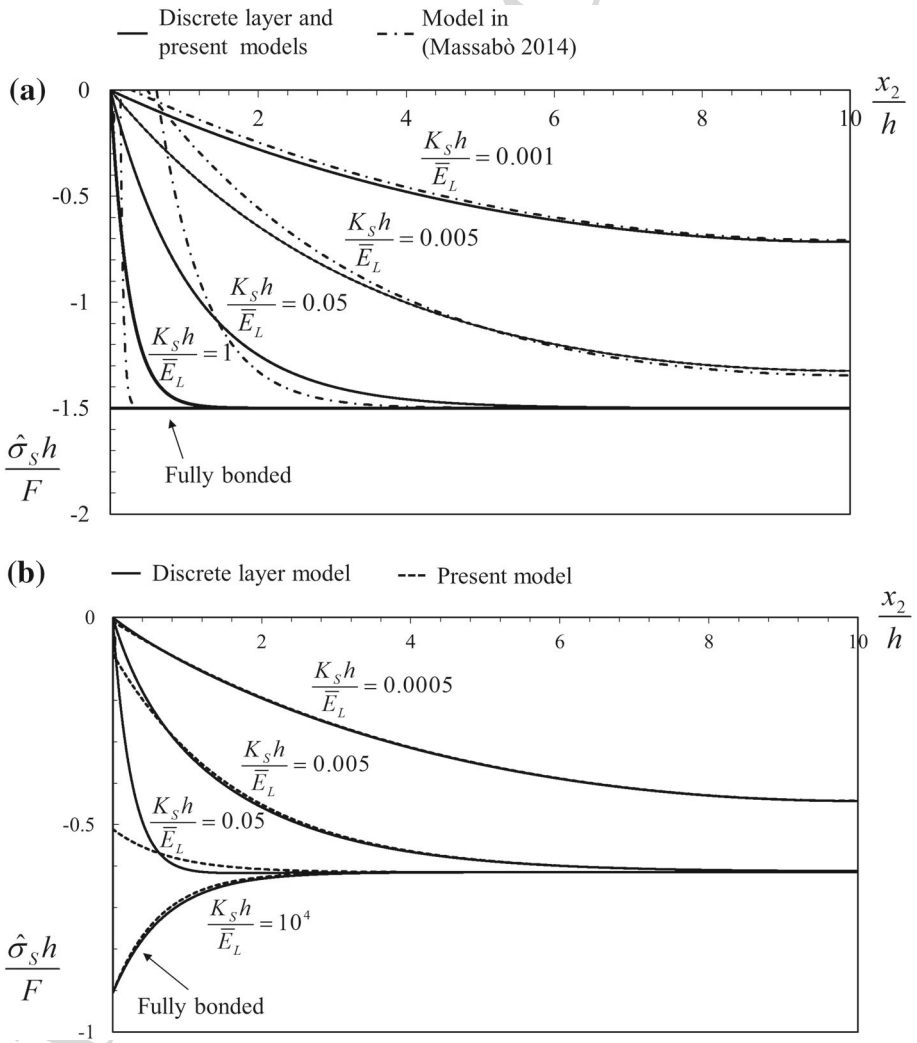

Fig. 11 Interfacial tractions along the length of a cantilever plate with $L/h = 10$, two equal thickness layers connected by a linear-elastic interface and subjected to a concentrated transverse force F at the free end (Fig. 10). The layer elastic constants: $E_T/E_L = 1/25$, $G_{LT}/E_L = 1/50$, $G_{TT}/E_L = 1/125$ and $\nu_{LT} = \nu_{TT} = 0.25$, and $\bar{E}_L = \bar{C}_{22} = E_L/(1 - \nu_{LT}\nu_{TL})$. **a** Stacking sequence (0, 0); solid lines: discrete layer and present models, dashed–dotted lines: model in Massabò (2014). **b** Stacking sequence (90, 0); solid lines: discrete layer model, dashed lines: present model

a larger mismatch of the interfacial stiffnesses, namely, for $K_S = 0$ and $G/G_{LT} = 0$, along the crack, and $1/K_S = 0$ and $G/G_{LT} = 1$, in the intact domain, the inaccuracy would substantially increase and the model predict an unrealistic linear deflection in the cracked and intact regions of the specimen (not shown). The results obtained with the homogenized structural model in Massabò and Campi (2014) are also shown in the figure and well reproduce the results of the discrete layer model.

The continuity condition imposed on the transverse shear forces at the crack tip cross sections and Eqs. (36) and (37) explain that the difference between the gradients of the transverse displacements in the two regions at $x_2 = a$, $w_{0,2}(a^+) - w_{0,2}(a^-)$, is controlled by the difference between

Journal: 41939 MS: 0032 TYPESET DISK LE CP Disp.:2018/8/24 Pages: 21 Layout: Large

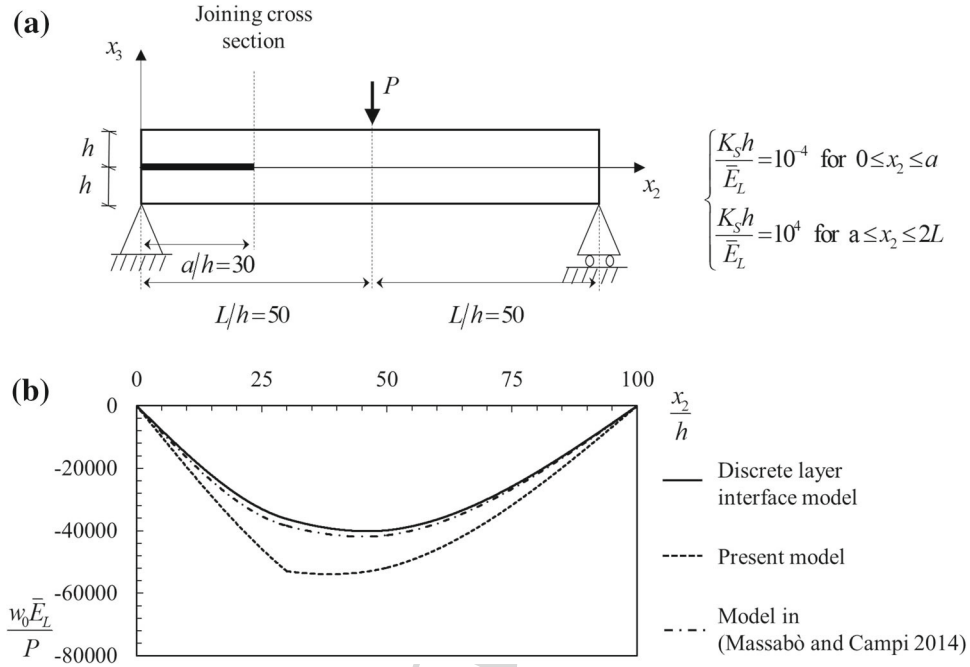

Fig. 12 **a** End Notched Flexural specimen with two equal thickness layers bonded by a linear-elastic interface with interfacial stiffnesses $K_S h/\bar{E}_L = 10^{-4}$ for $0 \le x_2 \le a$ and $K_S h/\bar{E}_L = 10^4$ for $a \le x_2 \le 2L$. **b** Deformed shape (shear correction factor $k_{44} = 5/6$)

the constants A^S_{44} of the two domains, which is given in Eq. (37) and depends on the difference between the homogenized shear rigidities. The kinematic continuity conditions, Eq. (34), do not enforce the gradients of the transverse displacements to coincide at continuity cross sections between different domains, as in classical structural theories, and impose instead a condition on the additional variable θ_2. The problem is not present in the homogenized model in Massabò and Campi (2014), where continuity conditions are applied also on the gradient of the transverse displacement, and this explains why results in Fig. 12b are accurate.

5 Conclusions

A homogenized structural model has been formulated for linear static analysis of multilayered beams and wide plates with layers joined by thin compliant interlayers, e.g., adhesive layers, or uniformly distributed mechanical connectors, e.g., nails, dowels, screws, pins, or stitches. The thin interlayers and the action of the connectors are described by introducing zero-thickness sliding interfaces, whose mechanical response is controlled by linear-elastic constitutive laws. The model extends the zigzag theory formulated in Tessler et al. (2009) for fully bonded beams to account for the presence of imperfect interfaces using the multiscale strategy proposed in Massabò and Campi (2014). The global displacement field of first-order shear deformation theory is enriched by a local field which describes the inhomogeneous material structure and the jumps at the imperfect interfaces. A homogenization technique based on the imposition of continuity conditions on the tractions at the layer interfaces is used to define the local variables in terms of the global variables. Homogenized equilibrium equations are then derived using a variational technique; they depend on four global variables, independently of the number of layers or imperfect interfaces in the system. The problem is solved in closed form, also in the limit of fully debonded layers; this allows to easily investigate and understand the effects of the status of the bonding on global and local fields.

The model formulated in this paper overcomes the limitations of models based on a discrete layer discretization of the problem, where the number of displacement variables depends on the number of layers and imperfect interfaces. It also has advantages over models which are based on a homogenized zigzag approach and describe the thin interlayers as regular layers, since the solution is more efficient and the model can treat systems made of individual layers joined by mechanical fasteners, where the actual thickness of the interfaces is zero. The model maintains the advantages of the original zigzag theory in Tessler et al. (2009) in the treatment of the shear deformations and is able to accurately predicts global and local fields in simply supported highly anisotropic thick plates, also in the presence of imperfect or fully debonded interfaces. It improves solutions obtained with homogenized structural models based on classical zigzag theories (Massabò and Campi 2014). Improvements with respect to similar homogenized approaches are also observed in the treatment of clamped supports, where the fictitious boundary layers observed in the previous works are reduced in size or

Journal: 41939 MS: 0032 TYPESET DISK LE CP Disp.:2018/8/24 Pages: 21 Layout: Large

not present. Important limitations are instead observed in the capability of the model to treat plates with in-plane discontinuities, such as finite length delaminations, for which other homogenized approaches prove to be more accurate.

The formulation is limited to beams or plates in cylindrical bending with layers aligned along the bending axes and linear elastic, sliding only, interfaces. The formulation can be extended to model 2D structures and interfaces with generally nonlinear traction laws, which are necessary to describe interfacial damage, delaminations, and problems, where the interfacial normal tractions are important, following the methodology in Massabò and Campi (2015).

Acknowledgements Support by the U.S. Office of Naval Research, Contract no. N00014-14-1-0254, program manager Dr. Y. D. S. Rajapakse and by the (MURST) Italian Department for University and Scientific and Technological Research, MIUR Prin15 Project 2015LYYXA8 are gratefully acknowledged.

Compliance with ethical standards

Conflict of interest On behalf of all authors, the corresponding author states that there is no conflict of interest.

Appendix A: Solutions for fully debonded layers

In a plate with fully debonded layers (very compliant interlayers or absence of mechanical connectors) with $K_S^i \to 0$ for $i = 1, \ldots, n-1$, $G \to 0$ and $G/K_S^i \to h/(n-1)$ from Eq. (19), the enrichment function, Eq. (22), becomes

$$ {}^{(k)}\phi(x_3) = -(x_3 - x_3^{k-1}) + \frac{h}{n-1}(k-1) - \sum_{i=1}^{k-1} {}^{(i)}h, \quad (44) $$

and the displacement field in terms of the global variables, Eq. (23), modifies as

$$ \begin{aligned} {}^{(k)}v_2(x_2, x_3) &= v_{02}(x_2) + [\varphi_2(x_2) - \theta_2(x_2)]x_3 + \theta_2(x_2) \\ &\left(x_3^{k-1} + \frac{h(k-1)}{n-1} - \sum_{i=1}^{k-1} {}^{(i)}h\right) \\ {}^{(k)}v_3(x_2) &= w_0(x_2). \end{aligned} \quad (45) $$

The strain and stress fields are obtained from Eqs. (24) and (25) setting $G \to 0$:

$$ \begin{aligned} {}^{(k)}\varepsilon_{22}(x_2) &= v_{02,2}(x_2) + \left[\varphi_{2,2}(x_2) - \theta_{2,2}(x_2)\right]x_3 + \theta_{2,2}(x_2) \\ &\left(x_3^{k-1} + \frac{h(k-1)}{n-1} - \sum_{i=1}^{k-1} {}^{(i)}h\right) \\ 2\,{}^{(k)}\varepsilon_{23}(x_2) &= \varphi_2(x_2) + w_{0,2}(x_2) - \theta_2(x_2) \\ {}^{(k)}\sigma_{22}(x_2, x_3) &= {}^{(k)}\bar{C}_{22}\Big\{v_{02,2}(x_2) + [\varphi_{2,2}(x_2) - \theta_{2,2}(x_2)]x_3 \\ &+\theta_{2,2}(x_2)\left(x_3^{k-1} + \frac{h(k-1)}{n-1} - \sum_{i=1}^{k-1} {}^{(i)}h\right)\Big\} \\ {}^{(k)}\sigma_{23}(x_2, x_3) &= {}^{(k)}C_{44}[\varphi_2(x_2) + w_{0,2}(x_2) - \theta_2(x_2)]. \end{aligned} \quad (46) $$

The equilibrium equation (38) and boundary conditions (39) are obtained by taking the limit of the coefficients in Eq. (37) as the interfacial stiffness goes to zero. For this limit, the constants A_{22}, B_{22}, and D_{22}, which are independent of the interfacial stiffness, do not change, while the remaining constants take the following forms:

$$ \begin{aligned} B_{22}^S &= -B_{22} + \sum_{k=1}^{n} {}^{(k)}\bar{C}_{22}{}^{(k)}h\left\{x_3^{k-1} + h\frac{k-1}{n-1} - \sum_{i=1}^{k-1} {}^{(i)}h\right\} \\ D_{22}^S &= -D_{22} + \sum_{k=1}^{n} {}^{(k)}\bar{C}_{22}\left\{x_3^{k-1} + h\frac{k-1}{n-1} - \sum_{i=1}^{k-1} {}^{(i)}h\right\}\int_{x_3^{k-1}}^{x_3^k} x_3 \mathrm{d}x_3 \\ D_{22}^{SS} &= -2D_{22}^S - D_{22} \\ &+\sum_{k=1}^{n} {}^{(k)}\bar{C}_{22}{}^{(k)}h\left\{x_3^{k-1} + h\frac{k-1}{n-1} - \sum_{i=1}^{k-1} {}^{(i)}h\right\}^2 \\ A_{44} &= \sum_{k=1}^{n} {}^{(k)}C_{44}{}^{(k)}h; \quad A_{44}^{SS} = -A_{44}^S = A_{44}; \quad \hat{A}_{44}^S = 0. \end{aligned} \quad (47) $$

In a plate made of layers having the same thickness, h/n, and elastic constants, the coefficients in Eq. (47) simplify. When the origin of the coordinate system is placed at the plate mid-thickness, they become

$$ \begin{aligned} &A_{22} = \bar{C}_{22}h; \quad B_{22} = 0; \quad D_{22} = \frac{\bar{C}_{22}h^3}{12}; \\ &A_{44} = -A_{44}^S = A_{44}^{SS} = C_{44}h; \quad \hat{A}_{44}^S = 0 \\ &B_{22}^S = 0; \quad D_{22}^S = \frac{\bar{C}_{22}h^3}{12n}; \quad D_{22}^{SS} = \frac{\bar{C}_{22}h^3}{6n(n-1)}. \end{aligned} \quad (48) $$

Appendix B: decoupled equilibrium equations

The equilibrium equation (38) is decoupled by subsequent derivations/substitutions and eliminating $w_{0,2}$ through the introduction of a variable γ given by $\gamma = \varphi_2 + w_{0,2}$. The

Journal: 41939 MS: 0032 TYPESET DISK LE CP Disp.:2018/8/24 Pages: 21 Layout: Large

system of decoupled equations, which has the same order of the original system, is

$$\theta_{2,222} + \frac{A_{44}a_2 + A^S_{44}}{A_{44}a_1}\theta_{2,2} + \frac{f_3 + k_{44}A_{44}a_{3,2}(x_2)}{k_{44}A_{44}a_1} = 0$$
$$\gamma = a_1\theta_{2,22} + a_2\theta_2 + a_3(x_2)$$
$$v_{02,22} = \frac{B_{22}D^{SS}_{22} - D^S_{22}B^S_{22}}{A_{22}D^S_{22} - B_{22}B^S_{22}}\theta_{2,22} - \frac{B_{22}(k_{44}A^{SS}_{44} + \hat{A}^S_{44})}{A_{22}D^S_{22} - B_{22}B^S_{22}}\theta_2$$
$$- \frac{k_{44}A^S_{44}B_{22}}{A_{22}D^S_{22} - B_{22}B^S_{22}}\gamma - \frac{D^S_{22}}{A_{22}D^S_{22} - B_{22}B^S_{22}}f_2$$
$$\varphi_{2,22} = \frac{(B^S_{22})^2 - A_{22}D^{SS}_{22}}{A_{22}D^S_{22} - B_{22}B^S_{22}}\theta_{2,22} + \frac{A_{22}(k_{44}A^{SS}_{44} + \hat{A}^S_{44})}{A_{22}D^S_{22} - B_{22}B^S_{22}}\theta_2$$
$$+ \frac{k_{44}A^S_{44}A_{22}}{A_{22}D^S_{22} - B_{22}B^S_{22}}\gamma + \frac{B^S_{22}}{A_{22}D^S_{22} - B_{22}B^S_{22}}f_2$$
$$w_{0,2} = \gamma - \varphi_2, \tag{49}$$

where

$$a_1 = \frac{B_{22}[B_{22}D^{SS}_{22} - D^S_{22}B^S_{22}] + D_{22}[(B^S_{22})^2 - A_{22}D^{SS}_{22}] + D^S_{22}[A_{22}D^S_{22} - B_{22}B^S_{22}]}{k_{44}A_{44}(A_{22}D^S_{22} - B_{22}B^S_{22}) + k_{44}A^S_{44}[(B_{22})^2 - A_{22}D_{22}]}$$
$$a_2 = \frac{[D_{22}A_{22} - (B_{22})^2][k_{44}A^{SS}_{44} + \hat{A}^S_{44}] - k_{44}A^S_{44}[A_{22}D^S_{22} - B_{22}B^S_{22}]}{k_{44}A_{44}(A_{22}D^S_{22} - B_{22}B^S_{22}) + k_{44}A^S_{44}[(B_{22})^2 - A_{22}D_{22}]}$$
$$a_3(x_2) = \frac{f_{2m}[A_{22}D^S_{22} - B_{22}B^S_{22}] + f_2[D_{22}B^S_{22} - B_{22}D^S_{22}]}{k_{44}A_{44}(A_{22}D^S_{22} - B_{22}B^S_{22}) + k_{44}A^S_{44}[(B_{22})^2 - A_{22}D_{22}]}. \tag{50}$$

The first equation (49) is a third-order differential equation in θ_2, whose solution allows cascading solutions for γ, through an algebraic equation, and for v_{02} and φ_2, through solutions of two second-order differential equations. The last equation (49), which is a first-order differential equation, defines w_0.

References

Abrate S, Di Sciuva M (2018) 1.16 multilayer models for composite and sandwich structures. In: Comprehensive composite materials II. Elsevier, Oxford, pp 399–425. https://doi.org/10.1016/B978-0-12-803581-8.09885-4

Adam C, Heuer R, Raue A, Ziegler F (2000) Thermally induced vibrations of composite beams with interlayer slip. J Therm Stress 23:747–772. https://doi.org/10.1080/01495730050192392

Adekola AO (1968) Partial interaction between elastically connected elements of a composite beam. Int J Solids Struct 4:1125–1135. https://doi.org/10.1016/0020-7683(68)90027-9

Aitharaju VR (1999) C^0 zigzag kinematic displacement models for the analysis of laminated composites. Mech Compos Mater Struct 6:31–56. https://doi.org/10.1080/107594199305647

Alfano G, Crisfield MA (2001) Finite element interface models for the delamination analysis of laminated composites: mechanical and computational issues. Int J Numer Methods Eng 50:1701–1736. https://doi.org/10.1002/nme.93

Allix O, Ladevèze P (1992) Interlaminar interface modelling for the prediction of delamination. Compos Struct 22:235–242. https://doi.org/10.1016/0263-8223(92)90060-P

Andrews MG, Massabò R, Cox BN (2006) Elastic interaction of multiple delaminations in plates subject to cylindrical bending. Int J Solids Struct 43:855–886. https://doi.org/10.1016/j.ijsolstr.2005.04.025

Andrews MG, Massabò R, Cavicchi A, Cox BN (2009) Dynamic interaction effects of multiple delaminations in plates subject to cylindrical bending. Int J Solids Struct 46:1815–1833. https://doi.org/10.1016/j.ijsolstr.2008.11.027

Andruet RH, Dillard DA, Holzer SM (2001) Two- and three-dimensional geometrical nonlinear finite elements for analysis of adhesive joints. Int J Adhes Adhes 21:17–34. https://doi.org/10.1016/S0143-7496(00)00024-5

Averill RC (1994) Static and dynamic response of moderately thick laminated beams with damage. Compos Eng 4:381–395. https://doi.org/10.1016/S0961-9526(09)80013-0

Bai JM, Sun CT (1995) The effect of viscoelastic adhesive layers on structural damping of sandwich beams. Mech Struct Mach 23:1–16. https://doi.org/10.1080/08905459508905225

Campi F, Monetto I (2013) Analytical solutions of two-layer beams with interlayer slip and bi-linear interface law. Int J Solids Struct 50:687–698. https://doi.org/10.1016/j.ijsolstr.2012.10.032

Carpenter WC, Barsoum R (1989) Two finite elements for modeling the adhesive in bonded configurations. J Adhes 30:25–46. https://doi.org/10.1080/00218468908048192

Cho M, Parmerter R (1993) Efficient higher order composite plate theory for general lamination configurations. AIAA J 31:1299–1306. https://doi.org/10.2514/3.11767

Cox BN (2005) Snubbing effects in the pullout of a fibrous rod from a laminate. Mech Adv Mater Struct 12:85–98. https://doi.org/10.1080/15376490490493899

Darban H, Massabò R (2017a) A multiscale structural model for cohesive delamination of multilayered beams. In: AIMETA 2017—Proceedings of the 23rd conference of the Italian association of theoretical and applied mechanics, pp 1785–1792. ISBN 978-889-42484-7-0

Darban H, Massabò R (2017b) Thermo-elastic solutions for multilayered wide plates and beams with interfacial imperfections through the transfer matrix method. Meccanica. https://doi.org/10.1007/s11012-017-0657-6

Di Sciuva M (1986) Bending, vibration and buckling of simply supported thick multilayered orthotropic plates: an evaluation of a new displacement model. J Sound Vib 105:425–442. https://doi.org/10.1016/0022-460X(86)90169-0

Di Sciuva M (1987) An improved shear-deformation theory for moderately thick multilayered anisotropic shells and plates. J Appl Mech 54:589–596. https://doi.org/10.1115/1.3173074

Di Sciuva M (1997) Geometrically nonlinear theory of multilayered plates with interlayer slips. AIAA J 35:1753–1759. https://doi.org/10.2514/2.23

Di Sciuva M (2016) First-order displacement-based zigzag theories for composite laminates and sandwich structures: a review. In: VII European congress on computational methods in applied sciences and engineering, Crete Island, Greece, 5–10 June 2016, pp 4528–4552

Di Sciuva M, Gherlone M, Librescu L (2002) Implications of damaged interfaces and of other non-classical effects on the load carrying capacity of multilayered composite shallow shells. Int J Nonlinear Mech 37:851–867. https://doi.org/10.1016/S0020-7462(01)00102-0

Edlund U, Klarbring A (1990) Analysis of elastic and elastic–plastic adhesive joints using a mathematical programming approach. Comput Methods Appl Mech Eng 78:19–47. https://doi.org/10.1016/0045-7825(90)90151-B

Foschi RO (1985) Wood floor behavior: experimental study. J Struct Eng 111:2497–2508. https://doi.org/10.1061/(ASCE)0733-9445(1985)111:11(2497)

Gelfi P, Giuriani E, Marini A (2002) Stud shear connection design for composite concrete slab and wood beams. J Struct Eng 128:1544–1550. https://doi.org/10.1061/(ASCE)0733-9445(2002)128:12(1544)

Girhammar UA, Gopu VKA (1993) Composite beam-columns with interlayer slip-exact analysis. J Struct Eng 119:1265–1282. https://doi.org/10.1061/(ASCE)0733-9445(1993)119:4(1265)

Girhammar UA, Pan DH (2007) Exact static analysis of partially composite beams and beam-columns. Int J Mech Sci 49:239–255. https://doi.org/10.1016/j.ijmecsci.2006.07.005

Goodman JR, Popov EP (1968) Layered beam systems with interlayer slip. J Struct Div 94:2535–2548

Groh RMJ, Tessler A (2017) Computationally efficient beam elements for accurate stresses in sandwich laminates and laminated composites with delaminations. Comput Methods Appl Mech Eng 320:369–395. https://doi.org/10.1016/j.cma.2017.03.035

Hansen SW, Spies RD (1997) Structural damping in laminated beams due to interfacial slip. J Sound Vib 204:183–202. https://doi.org/10.1006/jsvi.1996.0913

Heuer R, Adam C (2000) Piezoelectric vibrations of composite beams with interlayer slip. Acta Mech 140:247–263. https://doi.org/10.1007/bf01182514

Jain LK, Mai Y-W (1994) Analysis of stitched laminated ENF specimens for interlaminar mode II fracture toughness. Int J Fract 68:219–244. https://doi.org/10.1007/bf00013069

Lenci S, Clementi F, Warminski J (2015) Nonlinear free dynamics of a two-layer composite beam with different boundary conditions. Meccanica 50:675–688. https://doi.org/10.1007/s11012-014-9945-6

Lu X, Liu D (1992) Interlayer shear slip theory for cross-ply laminates with nonrigid interfaces. AIAA J 30:1063–1073. https://doi.org/10.2514/3.11028

Massabò R (2014) Influence of boundary conditions on the response of multilayered plates with cohesive interfaces and delaminations using a homogenized approach. Frattura ed Integrità Strutturale 2014:11. https://doi.org/10.3221/igf-esis.29.20

Massabò R (2017) Propagation of Rayleigh–Lamb waves in multilayered plates through a multiscale structural model. Int J Solids Struct 124:108–124. https://doi.org/10.1016/j.ijsolstr.2017.06.020

Massabò R, Campi F (2014) An efficient approach for multilayered beams and wide plates with imperfect interfaces and delaminations. Compos Struct 116:311–324. https://doi.org/10.1016/j.compstruct.2014.04.009

Massabò R, Campi F (2015) Assessment and correction of theories for multilayered plates with imperfect interfaces. Meccanica 50:1045–1071. https://doi.org/10.1007/s11012-014-9994-x

Massabò R, Mumm DR, Cox B (1998) Characterizing mode II delamination cracks in stitched composites. Int J Fract 92:1–38. https://doi.org/10.1023/a:1007520324207

Mi Y, Crisfield MA, Davies GAO, Hellweg HB (1998) Progressive delamination using interface elements. J Compos Mater 32:1246–1272. https://doi.org/10.1177/002199839803201401

Murakami H (1984) A laminated beam theory with interlayer slip. J Appl Mech 51:551–559. https://doi.org/10.1115/1.3167673

Murakami H (1986) Laminated composite plate theory with improved in-plane responses. J Appl Mech 53:661–666. https://doi.org/10.1115/1.3171828

Newmark NM, Siess CP, Viest IM (1951) Tests and analysis of composite beams with incomplete interaction. Proc Soc Exp Stress Anal 9:75–92

Oehlers DJ, Coughlan CG (1986) The shear stiffness of stud shear connections in composite beams. J Constr Steel Res 6:273–284. https://doi.org/10.1016/0143-974X(86)90008-8

Pelassa M, Massabò R (2015) Explicit solutions for multi-layered wide plates and beams with perfect and imperfect bonding and delaminations under thermo-mechanical loading. Meccanica 50:2497–2524. https://doi.org/10.1007/s11012-015-0147-7

Penumadu D (2018) Durability of US naval composites and sandwich structures: science framework considering multiscale response in harsh sea environment. In: Davies P, Rajapakse YDS (eds) Durability of composites in a marine environment, vol 2. Springer International Publishing, Cham, pp 59–74. https://doi.org/10.1007/978-3-319-65145-3_4

Reddy JN (1987) A generalization of two-dimensional theories of laminated composite plates. Commun Appl Numer Methods 3:173–180. https://doi.org/10.1002/cnm.1630030303

Schmidt R, Librescu L (1996) Geometric nonlinear theory of laminated anisotropic composite plates featuring interlayer slips. Nova J Math Game Theory Algebra 5:131–147

Tessler A, Di Sciuva M, Gherlone M (2009) A refined zigzag beam theory for composite and sandwich beams. J Compos Mater 43:1051–1081. https://doi.org/10.1177/0021998308097730

Vanderbilt MD, Goodman JR, Criswell ME (1974) Service and overload behavior of wood joist floor systems. J Struct Div 100:11–29

Xu R, Wu Y (2007) Static, dynamic, and buckling analysis of partial interaction composite members using Timoshenko's beam theory. Int J Mech Sci 49:1139–1155. https://doi.org/10.1016/j.ijmecsci.2007.02.006

Journal: 41939
Article: 32

Springer
the language of science

Author Query Form

Please ensure you fill out your response to the queries raised below and return this form along with your corrections

Dear Author

During the process of typesetting your article, the following queries have arisen. Please check your typeset proof carefully against the queries listed below and mark the necessary changes either directly on the proof/online grid or in the 'Author's response' area provided below

Query	Details required	Author's response
1.	Kindly check and confirm the citation in the sentence of "The zigzag theories offer a good compromise…"	
2.	Please confirm the all section headings are correctly identified.	
3.	Kindly provide editor names for Ref. Abrate and Di Sciuva (2018).	
4.	Kindly check and confirm the journal title in Ref. Massabò (2014).	